

AD-A268 130



DOCUMENTATION PAGE

Form Approved
OMB No. 0704-0188

Estimated to average 1 hour per response, including the time for reviewing instructions, searching existing data sources, gathering and reviewing the collection of information, sending comments regarding this burden estimate or any other aspect of this burden estimate to Washington Headquarters Services, Directorate for Information Operations and Reports, 1215 Jefferson Davis Highway, Suite 1204, Arlington, VA 22202-4302, and to the Office of Management and Budget, Paperwork Reduction Project (0704-0188), Washington, DC 20503.

2. REPORT DATE

1993

3. REPORT TYPE AND DATES COVERED

THESIS/DOSSERTATION

4. TITLE AND SUBTITLE

Propagation Characteristics of Mesoscale Convective Systems

5. FUNDING NUMBERS

6. AUTHOR(S)

Charles H. Pappas

7. PERFORMING ORGANIZATION NAME(S) AND ADDRESS(ES)

AFIT Student Attending: St Louis University

8. PERFORMING ORGANIZATION
REPORT NUMBER

AFIT/CI/CIA-93-021

9. SPONSORING / MONITORING AGENCY NAME(S) AND ADDRESS(ES)

DEPARTMENT OF THE AIR FORCE
AFIT/CI
2950 P STREET
WRIGHT-PATTERSON AFB OH 45433-776510. SPONSORING / MONITORING
AGENCY REPORT NUMBER

11. SUPPLEMENTARY NOTES

12a. DISTRIBUTION / AVAILABILITY STATEMENT

Approved for Public Release IAW 190-1
Distribution Unlimited
MICHAEL M. BRICKER, SMSgt, USAF
Chief Administration

12b. DISTRIBUTION CODE

13. ABSTRACT (Maximum 200 words)

93 8 19 033

93-19323



14. SUBJECT TERMS

15. NUMBER OF PAGES

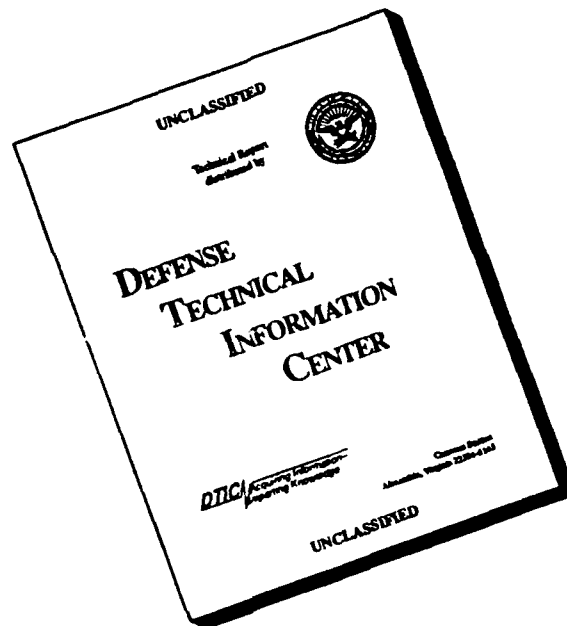
98

16. PRICE CODE

17. SECURITY CLASSIFICATION
OF REPORT18. SECURITY CLASSIFICATION
OF THIS PAGE19. SECURITY CLASSIFICATION
OF ABSTRACT

20. LIMITATION OF ABSTRACT

DISCLAIMER NOTICE



THIS DOCUMENT IS BEST
QUALITY AVAILABLE. THE COPY
FURNISHED TO DTIC CONTAINED
A SIGNIFICANT NUMBER OF
PAGES WHICH DO NOT
REPRODUCE LEGIBLY.

PROPAGATION CHARACTERISTICS OF MESOSCALE CONVECTIVE SYSTEMS

Charles H. Pappas, B.S.

Accession For	
NTIS CRA&I	<input checked="" type="checkbox"/>
DTIC TAB	<input checked="" type="checkbox"/>
Unannounced	<input type="checkbox"/>
Justification	
By	
Distribution /	
Availability Codes	
Dist	Avail and / or Special
A-1	

DTIC QUALITY INSPECTED 3

A Digest Presented to the Faculty of the Graduate School
of Saint Louis University in Partial Fulfillment of
the Requirements for the Degree of
Master of Science (Research)

1993

Digest

Case studies were undertaken on mesoscale convective systems (MCS) on an individual storm basis to examine factors influencing MCS propagation characteristics. This was done by examining numerous specific storms during a portion of the warm seasons (June-September) of 1990 through 1992. Three cases were presented in detail to illustrate the types of propagation typically exhibited by mesoscale convective systems. This research attempts to analyze why MCSs exhibit a particular type of propagation and if that propagation can be accurately predicted by forecasters on an operational basis.

Parameters such as moisture convergence, surface boundaries (fronts, dry lines, etc.), Convective Available Potential Energy (CAPE), equivalent potential temperature, vertical wind shear, and others were used in the diagnosis of a particular region where a storm grew and propagated toward.

The first case showed a storm located in Kansas propagating forward to the southeast. The second case study showed a MCS located in northern Texas displaying a very distinct backward (southwest) propagation toward the southwest. The third case focused on a MCS which exhibited quasi-stationary propagation along a cold front draped across northern Texas.

In the majority of the case studies, the correlation between the observed MCS propagation and the computed propagation was high. The propagation of the forward MCSs is more accurately described by using the 850-300 mb

average wind in the computations than the wind shear. The 850-300 mb wind shear vector results in a more accurate computed propagation vector for the backward propagating MCSs.

The role of high CAPE air, frontal boundaries, surface and 850 mb θ_e axes, and other parameters aided in determining the mode of propagation in many cases. Also, by comparing the storm-relative inflow vectors (having source regions upstream from the MCS) with the observed propagation vectors in all the case studies, it was found that they were anti-parallel in the majority of the cases. These upstream regions are the sources of moist and unstable air needed to sustain a MCS.

**PROPAGATION CHARACTERISTICS OF
MESOSCALE CONVECTIVE SYSTEMS**

Charles H. Pappas, B.S.

**A Thesis Presented to the Faculty of the Graduate School
of Saint Louis University in Partial Fulfillment of
the Requirements for the Degree of
Master of Science (Research)**

1993

COMMITTEE IN CHARGE OF CANDIDACY:

**Professor James T. Moore,
Chairperson and Advisor**

Professor Gandikota V. Rao

Assistant Professor Charles E. Graves

ACKNOWLEDGEMENTS

The author wishes to express deep appreciation to Dr. James T. Moore, advisor and chairman of the research committee (and all-around nice guy, WAG) for his patience, expertise, and many hours of *on-time* appointments while preparing this thesis. The author also wishes to express his appreciation to Dr. Charles E. Graves, (for the use of computer hardware and software), and Dr. Gandikota V. Rao for the effort and valuable time in reviewing this thesis. Also, I want to thank Ms. Andrea Hardy for her expertise in PC-McIDAS. Thank you to Sean Nolan for programming help. Thank you to Lt Col Chuck Benson for being a great commander. To the AFIT Team members, Rob and Mark, thanks for the laughs just when it all seemed overwhelming. Thank you United States Air Force for providing me with the opportunity to undertake this research after spending 15 months in Panama. To my parents, for instilling in me the confidence and drive to do more than I think I am able. Finally, and most importantly, to my beautiful wife Amy, for her continuous patience, love, and support through this project.

TABLE OF CONTENTS

Title	Page
1. Introduction and Objectives	1
a. Scientific Problem	1
b. Research Objective	2
2. Review of Related Literature	4
a. MCS Criteria/Definition	4
b. MCS Propagation	7
3. Research Methodology	21
a. Analysis Procedure	21
1) Satellite Imagery	21
2) Objective Analysis	23
b. Analytical Techniques	25
4. Discussion of Results	28
a. Case Study 1, Forward Propagating MCS	28
1. Description of the Event	28
2. Synoptic and Mesoscale Conditions	30
3. Definition of Backward-Relative and Forward- Relative Propagating Storms	37
4. Discussion of Propagation	39
b. Case Study 2 Backward Propagating MCS	42

TABLE OF CONTENTS (CONTINUED)

Title	Page
1. Description of the Event	42
2. Synoptic and Mesoscale Conditions	44
3. Discussion of Propagation	53
c. Case Study 3 Quasi-Stationary Propagating MCS	56
1. Description of the Event	56
2. Synoptic and Mesoscale Conditions	58
3. Discussion of Propagation	63
5. Composite Results	73
a. Deviation of Storm Motion from Mid-Tropospheric Mean Wind and Wind Shear	73
b. Computed Propagation Vectors vs Observed Propagation	74
1. Synoptic Environments for Propagation Modes	78
Forward	81
Backward	82
Quasi-Stationary	83
2. Storm-Relative Inflow Vectors	84
6. Associated Errors	87
7. Summary and Conclusions	89
BIBLIOGRAPHY	93
Vita Auctoris	98

LIST OF TABLES

Table	Page
1 Classification of meso-alpha scale weather systems.	5
2 Mesoscale convective complex physical characteristics.	6
3 Mesoscale convective system criteria.	24
4 Computed storm propagation using 850-300 mb average wind vs observed propagation.	76
5 Computed storm propagation using 850-300 mb wind shear vs observed propagation.	77
6 Comparison of storm motion with 850-300 mb average wind.	79
7 Comparison of storm motion with 850-300 mb wind shear.	80

LIST OF FIGURES

Figure	Page
1 Sketch of a convective storm in an environment where the wind veers with height. V_L and V_u are lower and upper environmental winds. Dashed arrows inside storm are mean of environmental winds.	9
2 Schematic representation of the flow at upper and lower levels, relative to a MCS represented by a cylinder. Plus and minus signs indicate positive or negative non-hydrostatic pressures.	9
3 Hodograph showing direction of Mesoscale Beta Element (MBE) movement relative to 850 and 300 mb wind vectors and the mean tropospheric wind vector.	12
4 Schematic of thunderstorm propagation with cells forming on the left and moving from left to right creating a multicell thunderstorm complex.	13
5 Showing how the development (decay) of new cells on the right (left) flank causing the cluster to move to the right of the wind.	14
6 Patterns of 850 mb θ_e ridge axes associated with MCS development and propagation.	18
7 The MB enhancement curve.	22
8 Satellite IR image for 09 UTC 5 June 1991.	29
9 Same as Fig. 8, except for 11 UTC.	29
10 Same as Fig. 8, except for 12 UTC.	31
11 Same as Fig. 8, except for 14 UTC.	31
12 Surface weather map for 00 UTC 5 June 1991.	32

LIST OF FIGURES (CONTINUED)

Figure	Page
13 Composite chart for 00 UTC 5 June 1991.	33
14 Equivalent potential temperature chart for 00 UTC 5 June 1991.	35
15 Same as Fig. 9, except for 12 UTC 5 June 1991.	36
16 Same as Fig. 10, except for 12 UTC 5 June 1991.	36
17 Same as Fig. 11, except for 12 UTC 5 June 1991.	38
18 Example of a propagation vector plot for a backward-relative propagating MCS.	40
19 Same as in Fig. 18, except for forward-relative propagating MCS.	40
20 Propagation vector plot for 5 June 1991 MCS.	41
21 Storm-relative inflow vector plot for Little Rock, Arkansas for 5 June 1991.	41
22 Same as in Fig. 21, except for Norman, Oklahoma.	43
23 Same as in Fig. 21, except for Monett, Missouri.	43
24 Same as in Fig. 12, except for 12 UTC 10 September 1992.	45
25 Same as in Fig. 13, except for 12 UTC 10 September 1992.	46
26 300 mb isotachs for 12 UTC 10 September 1992. Arrows indicate direction of wind flow.	46
27 (A) 850 mb moisture convergence for 12 UTC 10 September (B) same as (A), except for θ_e .	47

LIST OF FIGURES (CONTINUED)

Figure	Page
28 Satellite image for 21 UTC 10 September 1992.	49
29 Surface weather map for 00 UTC 11 September 1992.	50
30 Surface dewpoint analysis for 11 September 1992.	50
31 Surface θ_e analysis for 00 UTC 11 September 1992.	51
32 As in Fig. 27b, except for 00 UTC 11 September 1992.	51
33 As in Fig. 25, except for 00 UTC 11 September 1992.	52
34 Storm-relative inflow vector plot for Del Rio, Texas for 11 September 1992.	54
35 Same as in Fig. 34, except for Midland, Texas.	54
36 Same as in Fig. 34, except for El Paso, Texas.	55
37 Propagation vector plot for 11 September 1992 MCS.	55
38 Satellite IR image for 02 UTC 11 September 1992.	57
39 Surface weather map for 21 UTC 15 June 1992.	59
40 As in Fig. 39, except for 00 UTC 16 June 1991.	60
41 Surface moisture divergence chart for 00 UTC 16 June 1992.	61
42 Composite chart for 00 UTC 16 June 1992.	61
43 θ_e analysis for 00 UTC 16 June 1992.	62
44 Convective stability analysis for Topeka, Kansas for 00 UTC 16 June 1992.	64

LIST OF FIGURES (CONTINUED)

Figure	Page
45 Skew-T Log P diagram for Topeka, Kansas at 00 UTC 16 June 1992.	65
46 Satellite IR image for 21 UTC 15 June 1992.	66
47 As in Fig. 45, except for 23 UTC 15 June 1992.	66
48 As in Fig. 45, except for 00 UTC 16 June 1992.	67
49 As in Fig. 45, except for 03 UTC 16 June 1992.	67
50 Propagation vector plot for 16 June 1992 MCS.	69
51 Storm-relative inflow vector plot for Topeka, Kansas for 16 June 1992.	69
52 As in Fig. 51, except for Dodge City, Kansas.	70
53 As in Fig. 51, except for Norman, Oklahoma.	70
54 As in Fig. 43, except for 12 UTC 16 June 1992.	71
55 (a) Scatter diagram for the deviation of the storm motion from the 850-300 mb average wind. Axes are the deviation in the u and v directions (b) same as in (a), except for 850-300 mb wind shear.	75

1. INTRODUCTION and OBJECTIVES

Mechanisms which exert control on Mesoscale Convective Systems (MCS) initiation and propagation must be understood in order to accurately forecast their movement and propagation. MCSs are not simply advected along by the mean cloud-layer tropospheric wind, but rather, the movement is a complicated fashion through a combination of environmental and storm-scale interactions between the properties associated with the MCS and those of the near-environment.

a. Scientific Problem

Forecasters face difficulty when predicting the propagation and movement of MCSs. It is difficult to conceptualize the exact role that environmental parameters, such as vertical wind shear and moisture convergence, play in determining the type of storm propagation exhibited. Since MCSs are a common seasonal feature in the mid-latitudes, it is very important that these systems and their associated weather phenomena be forecast with increased confidence and accuracy. The location of natural disasters associated with MCSs, such as flash flooding and tornadoes, have a better likelihood of being predicted more precisely if forecasters know in which direction the parent storm will propagate. Propagation is an important factor to consider when forecasting severe weather and heavy rainfall associated with convection.

The type of MCS, its level of severity, direction and speed of propagation are all strongly dependent on the environmental conditions into which the storm moves. For example, vertical wind shear and buoyancy play key roles in storm initiation and propagation. Buoyancy is the controlling factor in an air parcel's ability to accelerate vertically. More importantly, vertical wind shear influences the form that the convection may take (e.g., supercell, multicell, squall line, etc.) as well as the movement of the convective system. Knowledge of the effects of local mesoscale variations or terrain features on storm structure and evolution is limited. However, their importance to forecasting is undeniable (Weisman and Klemp 1986).

MCSs play a major role in controlling precipitation events in the Midwestern United States. During the warm season months, they can account for up to 50% or more of the rainfall over much of the region between the Rocky Mountains and the Mississippi River (Fritsch et al. 1986). As well as being important precipitation producers, MCSs can be responsible for severe weather. One quarter of all MCC events result in human death or injury (Maddox 1983).

b. Research Objective

The objective of this thesis is, through the examination of numerous specific case studies, to examine why MCSs exhibit a particular type of propagation in the central United States, and if this propagation may be accurately predicted by forecasters using an operational database. In order to

understand how a MCS propagates in a given fashion, it is necessary to examine the synoptic environments in which the MCS grows and propagates toward. This study includes a forward propagating storm as the first case study. The second case study examines a backward propagating storm, and the third case examines a quasi-stationary propagating storm. We attempt to characterize various environments which dictate whether a MCS will move forward, backward or remain quasi-stationary.

2. REVIEW OF RELATED LITERATURE

The goal of this research is to build on previous research on convective storm propagation by computing propagation and storm-relative inflow vectors and characterizing the environment which favors a certain type of storm propagation over another. The net result will be to develop physical models which may aid forecasters in determining the type of propagation (forward, backward, or quasi-stationary) and the direction of propagation in an operational environment.

a. Mesoscale Convective System Definition

Zipser (1982), defines MCSs as cloud and precipitation systems, with time and space scales of 3-12 hours and 20-500 km, respectively, together with their associated circulation systems, which include a group of cumulonimbus (Cb) clouds during most of the lifetime of the system. The Cb cloud group must exist for several lifetimes of its constituent clouds (at least 2 hours), and the Cb group must contribute at some time to a common upper tropospheric shield of outflow air. Also, deep convection must exist during some part of its lifetime. The mesoscale convective weather systems, as described by Maddox (1980), are presented in Table 1. Maddox's (1980) criteria of a Mesoscale Convective Complex (MCC), (a subset of MCSs), is presented in Table 2.

Almost all severe local storm and MCS events are associated with deep convection. To achieve deep convection, there are three necessary ingredients

TABLE 1. Classification of Meso- α scale, convectively driven weather systems according to physical characteristics, organization, and location (after Maddox 1980).

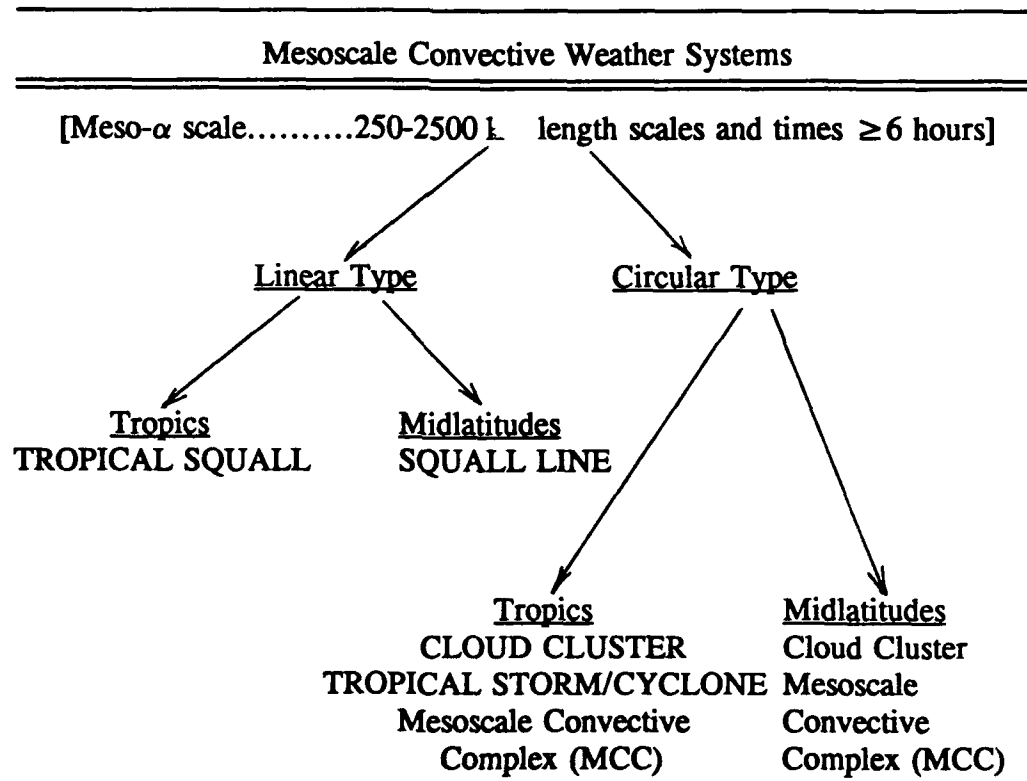


TABLE 2. Mesoscale Convective Complex (MCC)
(based upon analyses of enhanced IR satellite
imagery) (after Maddox 1980)

Physical Characteristics	
Size:	A-Cloud shield with continuously low IR temperature $\leq -32^{\circ}\text{C}$ must have an area $\geq 100,000\text{ km}^2$ B-Interior cold cloud region with temperature $\leq -52^{\circ}\text{C}$ must have an area $\geq 50,000\text{ km}^2$
Initiate:	Size definitions A and B are first satisfied
Duration:	Size definitions A and B must be met for a period ≥ 6 hours
Maximum extent:	Continuous cold cloud shield (IR temperature $\leq -32^{\circ}\text{C}$) reaches maximum size
Shape:	Eccentricity (minor axis/major axis) ≥ 0.7 at time of maximum extent
Terminate:	Size definitions A and B no longer satisfied

(as described in Doswell 1987): a) a moist layer of sufficient depth in the low or mid troposphere; b) a steep enough lapse rate to allow for a substantial positive area (on a sounding); and c) sufficient lifting of a parcel from the moist layer to allow it to reach its level of free convection (LFC). Moisture, conditional instability, and lifting are all necessary and each effects the convective potential in a different way.

According to Johns and Doswell (1992), in order to assess the potential for deep convection, a forecaster must be able to diagnose the current thermodynamic structure of the troposphere. The changes resulting from thermal advection and vertical motion fields must also be forecast as well.

b. MCS Propagation

Propagation refers to the movement of a thunderstorm or MCS as a result of preferred new cell development on one flank of the updraft. Propagation occurs because of a storms' interactions with an environment possessing potential buoyant energy and moisture convergence. In one example, the climatology of supercell storms demonstrates that many supercells move to the right of the mean wind and at a slower speed; hence it may be possible to forecast supercell motion to be at some fixed deviation from the mean wind (Doswell 1991).

Storm propagation is one of many influences on storm motion. It can speed up or slow down a MCS depending on whether the propagation is occurring on a forward or rear flank of the system (Chappell 1986). Storm

propagation can be forward, backward, stationary, or any combination of these three. If the propagation vector is directed opposite to the mean motion of the cells within the storm, a stationary or quasi-stationary MCS may result. A MCS which propagates forward may have its propagation vector aligned parallel to the cell vector so that the MCS may move faster than the environmental winds supporting the system.

The propagation of MCSs has been a focus of study in the recent literature. Doswell (1985) considers two ways to induce new development of updrafts and cause a storm to move via propagation. The first way includes the physical processes created by the storm itself. The up- and downdrafts, gust fronts, hydrometeors, release of latent heat, etc., can have effects within the storm and its immediate environment. These influences can enhance or suppress new updrafts and convection in certain locations. Newton and Newton (1959) suggest that the vertical transport of momentum could result in the storm behaving as if it were an "obstacle" to the environmental flow field. The storm is not literally a solid obstacle, but the large horizontal momentum gradients resulting from convection in a sheared environment produces non-hydrostatic pressures at any level acting to generate new convection on specific flanks of a storm. For example, in Fig. 1, this is the right-hand flank, relative to the mean wind in the cloud layer. These non-hydrostatic pressures can produce vertical accelerations independent of and comparable in strength to ordinary buoyancy forces (see Fig. 2). These are the perturbation pressure gradient forces.

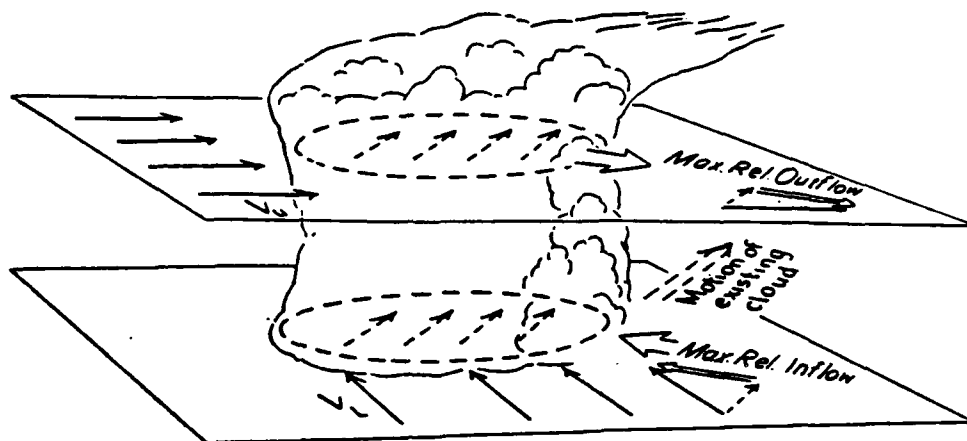


Figure 1. Sketch of a convective storm in an environment where the wind veers with height. V_L and V_u are lower and upper environmental winds. Dashed arrows inside storm is mean of environmental winds. (Newton 1960).

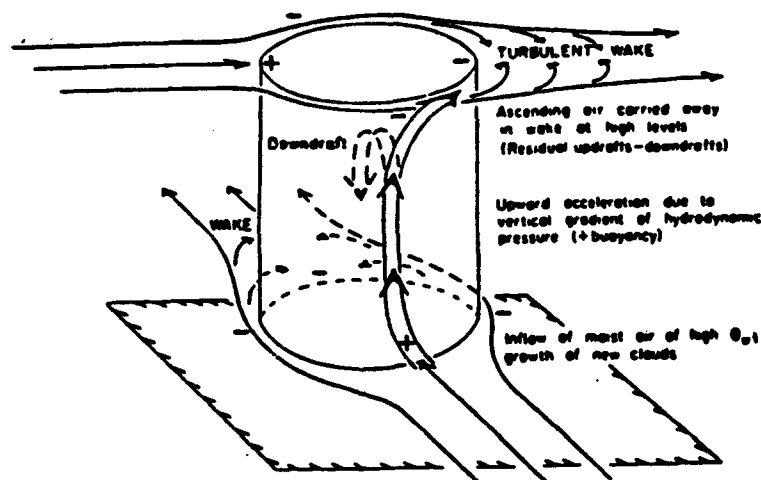


Figure 2. Schematic representation of the flow at upper and lower levels, relative to a rainstorm (MCS) represented by a cylinder. Plus and minus signs indicate positive or negative non-hydrostatic pressures. On the near side of the storm positive pressure is found in lower levels beneath a pressure deficit at upper levels. This indicates an upward acceleration (Newton and Newton 1959).

According to Newton and Newton (1959), the magnitude of these forces increases with storm diameter. Thus, the tendency for a storm to move to the right of the mean wind as a result of new convective growth on its right flank should be greatest when the storm diameter is large and the veering of the wind with height is strong.

The second way in which storm propagation may be influenced includes physical processes which are independent of the actual convective storm itself. It must be pointed out that the convective storm may interact with these processes and alter them drastically after storm initiation. An example of this was described by Browning (1965a) in which convective storms commenced their deviate motion upon encountering a warm front at the surface. Recently, gravity waves have been suggested by some authors to have a role in thunderstorm propagation. Although not proven, it is an interesting aspect of storm scale processes to consider.

In studying deviate thunderstorm motion which is obviously associated with some external mechanism, one of two things must be occurring: 1) internal mechanisms must be too weak, or below some threshold, to be effective at influencing storm motion, or 2) internal mechanisms must be in phase with an external process(es). More than likely, in the real world, there is a combination of external and internal mechanisms and processes (Doswell 1985).

Merritt and Fritsch (1984) presented a technique for determining the mean movement of heavy precipitation areas ($VIP \geq 3$ or coldest storm tops in Infrared (IR) satellite imagery) in MCCs, which they termed Mesoscale Beta

Elements (MBE). Based on an analysis of over 100 documented MCC and MCC-like events, they determined that MBE movement was best described by the same direction of the 850-300 mb mean cloud-layer shear vector (which is coincident with the dashed 850-300 mb thickness contours in Fig. 3), with as little as 10° difference between the two. The speed of the MBE appeared to be modulated by the strength and relative position of the low-level moisture convergence field.

Doswell's (1985) schematic model of storm propagation (see Fig. 4) detailed how new cells develop and grow taller as they approach and finally merge with the maturing cells. Eventually, precipitation forms in the main updraft and is held aloft temporarily while the cell matures.

Storms can either propagate discretely or continuously in a given direction. Newton and Frankhauser (1975) pointed out that discrete propagation requires the formation of new convective cells, and usually south and about 4-10 km away from the main storm complex, which will usually merge with the main storm in time (see Fig. 5). According to Browning (1964), continuous propagation is associated with new convective cells forming directly adjacent to the main updraft, continuously feeding it, where there is no distance separating the main storm from new cells.

In their study, Kane et al. (1987), found the -52° C cold-cloud shield centroid (as noted on a MB-enhanced IR image), provided a better correlation with the center of rainfall areas than the -32° C cold cloud shield centroid. In particular, the -52° C centroid track tended to bisect the rainfall area.

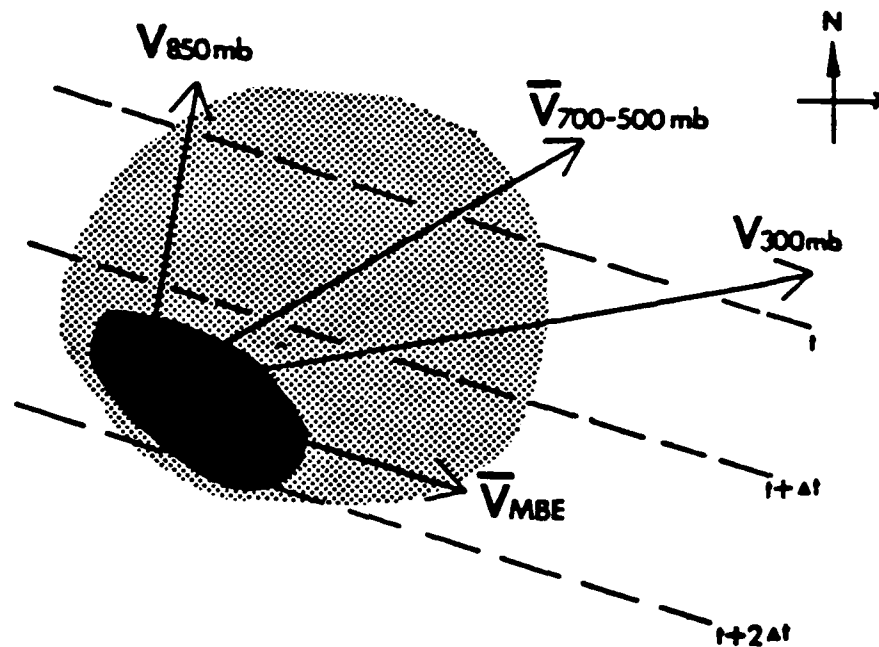


Figure 3. Schematic hodograph showing the direction of the Mesoscale Beta Element (MBE) movement relative to the 850 and 300 mb wind vectors and the mean tropospheric wind vector ($V_{700-500mb}$); dashed lines are the 850-300 mb thickness contours; light stippling is the $\leq -32^\circ \text{C}$ cold cloud shield of the MCC; black area is region of the MBEs (Merritt and Fritsch 1984).

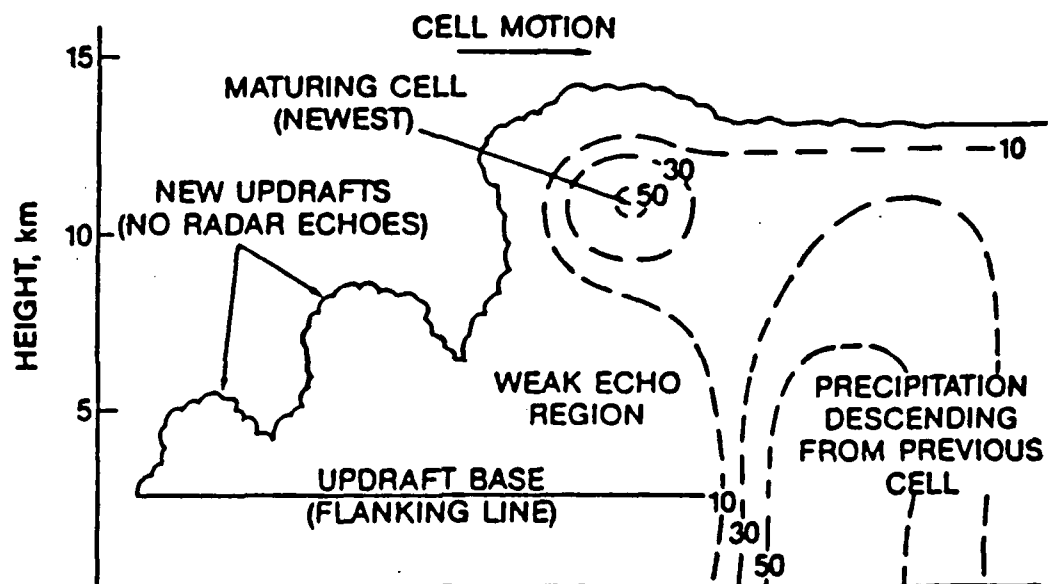


Figure 4. A schematic of thunderstorm propagation with cells, forming on the left of the figure and moving from the left to the right, creating a multicell thunderstorm complex. Dashed lines represent radar reflections of 10, 30, and 50 dBZ (Doswell 1985).

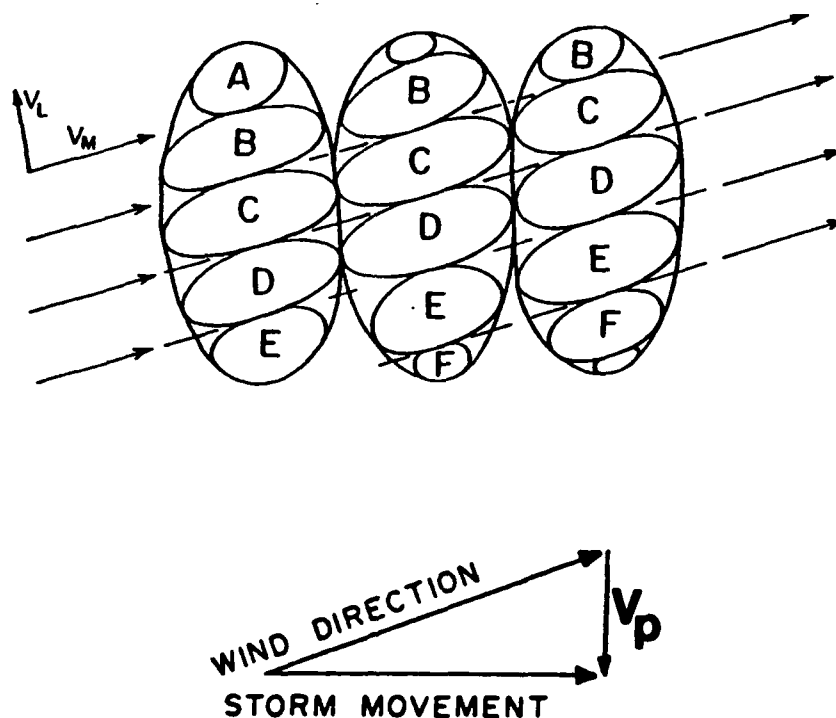


Figure 5. Diagram shows how the development of new cells on the right flank and the decay of old cells on the left flank cause the cluster as a whole to move to the right of the wind. Vectors represent lower tropospheric (V_L) and midtropospheric (V_M) winds relative to ground. Positions of lettered cells are at three successive times ~ 15 minutes apart. Cells A and B dissipate while F develops. The propagation effect is discrete. It occurs in a series of separate steps, each associated with new cell formation. V_p is propagation vector (Browning and Ludlam 1960).

Moreover, it did it in such a manner that the heaviest rainfall was usually slightly to the right of the path of the centroid. Knowledge of this relationship may be helpful for short term forecasting of storm propagation.

Newton and Frankhauser (1964) examined typical squall line situations where the wind veered strongly with height and found that individual convective storms may move as much as 60° to the right or 30° to the left of the direction of the mean wind in the cloud layer. Their results showed that radar echoes having the largest diameters moved farthest to the right of the mean wind.

Among the factors which may influence the patterns of development and propagation of convective storms is the distribution of stability and moisture and the fields of divergence and vertical motion. These physical processes are imposed on the storm by external sources and also generated by the convection itself. Newton and Katz (1958) and Newton and Newton (1959) indicated that large thunderstorm clusters moved systematically with an appreciable component toward the right of the upper-level winds. If the air within a thunderstorm (as part of a MCS) were to be drawn into the storm in equal quantities from upper and lower levels of the troposphere and mixed vertically by the up- and downdrafts, the mean horizontal motion inside the storm would correspond to the mean of the environmental winds through the layer in which the storm is imbedded (Newton and Frankhauser 1964). If, as is more realistic, most of the in-cloud air originates in the lower levels, the motion of the storm must be biased toward the velocity of the lower levels. By this consideration, a storm in which propagation plays a **minor** role should move toward the left of the

mean wind velocity, when the wind veers with height. The persistence of a convective storm depends on its velocity relative to the most unstable and moist air of the lower levels. There is a great deal of apparently random departure from the expected behavior described. Indications are that forecasting individual storm propagation must depend on a combination of physical considerations and statistical-empirical findings. Each storm should be treated as an individual case, since different storms under the same environmental conditions may propagate in different ways.

Along another line, Weaver (1979) put forth that the predominant theme throughout most of the literature regarding mechanisms of storm propagation related new cell development exclusively to features such as micro-cold fronts, updraft rotation, etc. He pointed out that these factors are important to storm propagation, but another significant source of deviate motion may be found in the pre-existing synoptic and subsynoptic boundary layer features. He presented a case study in which a radar echo expanded slowly northeastward with time, but the most intense radar reflectivity core remained nearly stationary on the west and southwest flank of the storm because it was essentially "anchored" to a frontal convergence zone. He speculated that most often, storm motion is a blending of three factors: 1) mean cloud layer wind, 2) boundary layer convergence zones, and 3) thunderstorm-induced convergence features.

Funk (1991), in an article about heavy convective rainfall forecasting techniques, covered the importance of low-level equivalent potential temperature (θ_e) as a thermodynamic property dependent on moisture and temperature, where

higher values represent a warmer and/or wetter air mass that is more conducive to convective development. A region of high θ_e air may also be the source of 'fuel' for MCS sustenance and may be an important factor in influencing which type of propagation a MCS may exhibit. Juying and Scofield (1989) and Shi and Scofield (1987) have shown that warm sector convection often develops near or along the θ_e ridge axis at 850 mb in the presence of unstable air and a lifting mechanism. Assuming that the upstream instability and low-level inflow directed toward the convective system are maintained, the convection may either: 1) propagate upstream along the ridge axis toward higher values of θ_e air, or 2) propagate downstream with moderate-to-strong middle-level winds but with possible regenerative cells developing within the higher θ_e air upwind of the convective storm (see Fig. 6).

In an effort to investigate the dynamic character of convective storms, Klemp and Wilhelmson (1978), developed a three-dimensional cloud model which simulated self-sustaining right- and left-moving storms which arose from the splitting of an original storm. Using one-directional wind profiles, they found that the tendency of an initial storm to split into two self-sustaining storms was strongly dependent on the intensity and distribution of the low level shear. For a right-moving storm, the downdraft was located along the left flank and the outflow near the ground spread out underneath the updraft. This forced continuous uplifting of the moist low-level inflow along its right flank. In this manner, the storm maintained its moisture supply and tended to propagate to its right.

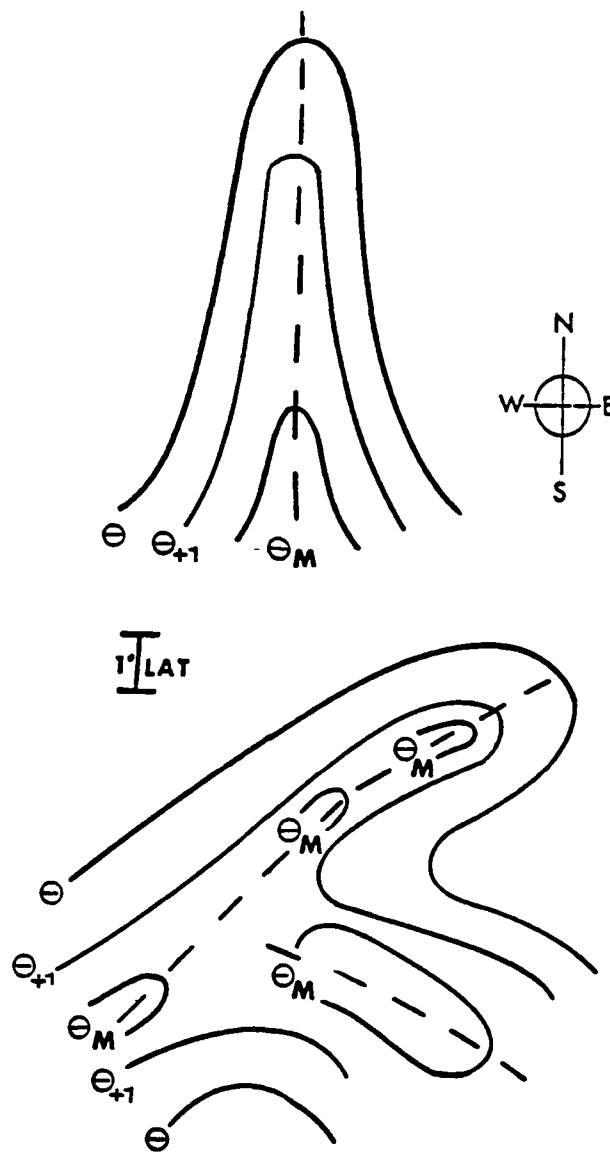


Figure 6. Patterns of low-level (850 mb) θ_e ridge axes associated with MCS development and propagation. MCSs develop and move along or near θ_e axis and θ_M where destabilization processes are taking place. Dashed line is axis of θ_e and θ_M is the θ_e maximum value (Juying and Scofield 1989).

Their simulations suggested how the environmental wind shear can determine whether a right- or left-moving storm could actually be produced by a particular sounding (hodograph). Curvature of the wind hodograph appeared to cause a relative enhancement of one of the downdrafts which in turn increased the gust-front-induced convergence beneath the storm. In particular, if the wind hodograph turned clockwise with height, development of the right-moving storm was enhanced, while if it turned counter-clockwise the left-moving storm was favored (Klemp and Wilhelmson 1978).

Roadcap and Rao (1993) studied the dependence of orientation, growth rate and horizontal and vertical extent of convection bands over the Arabian Sea on vertical shear, static stability and latent heat release from preexisting convection. Model output from their study showed that cloud growth in this region depended on the conditionally unstable stratification, while the orientation of the convective bands showed a sensitivity to the wind profile. They showed that the phase speed of the convective bands were dependent on precipitation efficiency and, in some cases, the longitudinal orientation of the bands were aided by the energy of the low-level flow.

The research presented in this chapter underscores the importance of examining and evaluating many processes and parameters associated with the synoptic/mesoscale environment and the MCS. As discussed above, both internal and external processes associated with the storm complex may affect its propagation. This research will concentrate on describing those external mechanisms affecting storm propagation resolved by synoptic scale datasets and

satellite imagery.

3. RESEARCH METHODOLOGY

This section describes the datasets, the analysis procedures, and analytical techniques used in the study. Emphasis is placed on describing the storm, cell, and propagation vector computation from the satellite imagery and upper air wind data.

a. Analysis Procedure

1. Satellite Imagery

The main source for satellite imagery data collection was PC-McIDAS. All the satellite imagery was gathered, examined, and archived using that system. Infrared (IR) imagery was collected at one hour intervals from the GOES satellite. The GOES MB enhancement curve (Fig. 7) was used to identify the convective elements ($\leq -52^{\circ}$ C) and to track the storm movement over time. The criteria for selecting MCS cases was based solely on physical characteristics observable in the MB-enhanced IR satellite imagery. Cold IR cloud tops are often associated with deep precipitating convective clouds (Follansbee and Oliver 1975), and so our requirement that large areas have a temperature $\leq -52^{\circ}$ C ensures that the system is active and that precipitation is falling over a large area (Maddox 1981). As Doswell (1984) points out, any categorization scheme involves some sort of arbitrary segregation. Obviously, the atmosphere does not recognize arbitrary categories (Bartels et al. 1984).

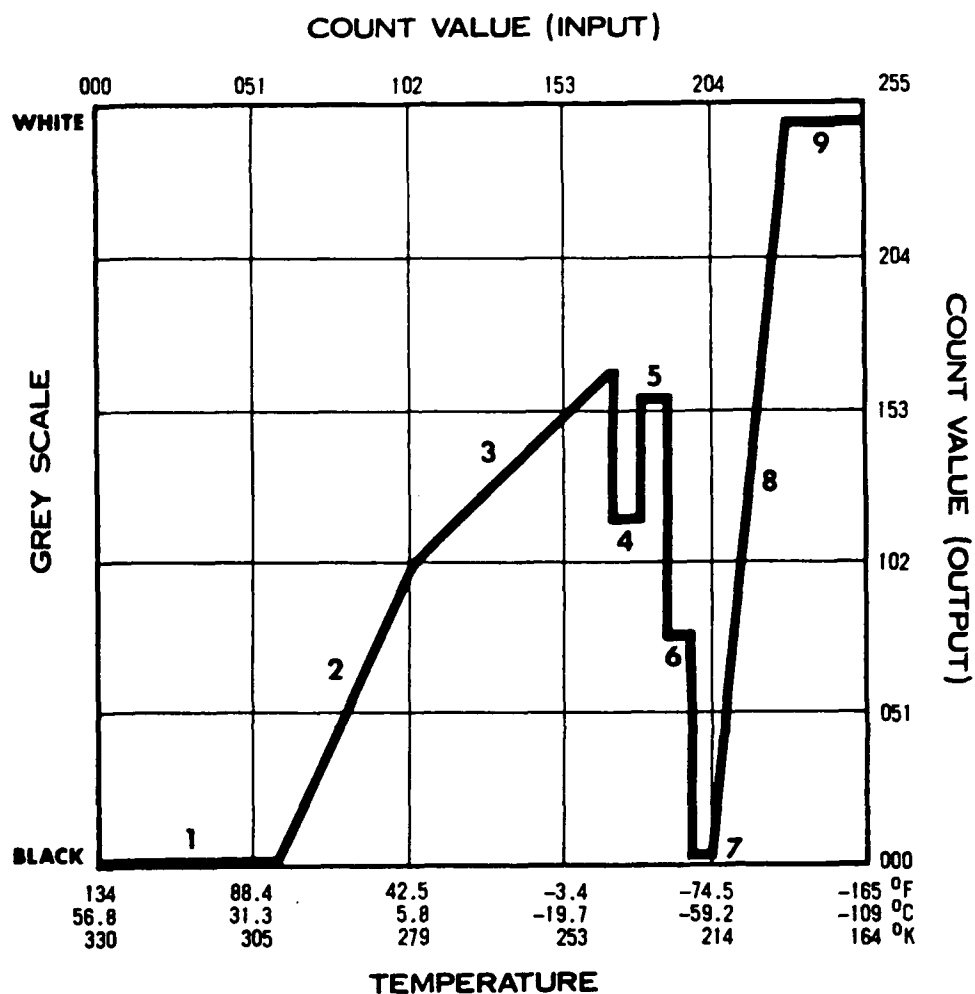


Figure 7. The MB enhancement curve. The solid line is a graph of temperature versus shading of this curve. The MB curve is meant to show overshooting tops of thunderstorms so the real enhancement starts at the cirrus cloud level (-32.2° C). Segments 4 through 7 contour convective areas. Segment 8 allows for good definitions of very cold domes (GOES User's Guide, 1983).

The satellite imagery loops were built to track MCSs and were centered around 00 and 12 UTC in order to take advantage of the availability of large datasets (rawinsonde data, hodographs, etc.) which aided characterizing the pre-storm and storm propagation environments. Cloud top temperatures $\leq -52^{\circ}\text{C}$ were chosen to represent the convective storm elements within the MCS in accordance with the convective characteristics noted by Maddox (1980), Kane et al. (1987), and Bartels et al. (1984). In their study, Kane et al. (1987) found the -52°C cold-cloud shield centroid track tended to bisect the rainfall area and that the heaviest rainfall was usually slightly to the south of the -52°C temperature axis of the MCS. The -52°C cold cloud top isotherm is conveniently represented by the MB-enhancement curve on the GOES satellite.

Bartels et al. (1984) states that not all MCSs meet the MCC criteria put forth by Maddox (1980) either due to size or time limitations. Their MCS criteria is presented in Table 3. Termed as a 'non-MCC', each MCS was subdivided into two categories. 'Small' MCSs generally have a $\leq -52^{\circ}\text{C}$ area, at maximum extent, of between 40,000 and 100,000 km^2 and they appear in satellite imagery as a 'mini-MCC'. 'Large' MCSs generally have areas of $\leq -52^{\circ}\text{C}$, at maximum extent, greater than 115,000 km^2 . We adopted this convention, and categorized our MCS cases as either small or large.

2. Objective Analysis

To be able to compute the essential wind and thermodynamic fields it is first necessary to objectively assign the data to specific data points. The grid

TABLE 3. Mesoscale Convective System Criteria
(Based on analysis of enhanced IR satellite imagery)
(after Bartels et al. 1984)

Characteristic	Criterion
Length:	Length scale of the $\leq -52^{\circ}$ C contiguous enhanced area on satellite image is ≤ 250 km
Duration:	Minimum length scale is maintained for at least 3 hours
Initiation:	Length scale criterion is first met
Maximum extent:	Contiguous cold cloud shield (IR temperature $\leq -52^{\circ}$ C) reaches maximum size
Termination:	Length scale criterion is no longer met

used in this study is 31 (x axis) columns by 21 (y axis) rows and the distance between each point on the upper air grid is 190.5 km true at 60 degrees North on a 1:15 million polar stereographic map. The distance between each point on the surface grid is 95.25 km. Data were interpolated to each point using the Barnes (1973) scheme. For the interpolations, the weighting function constants κ and γ for the upper air data were chosen to be 81,900 km² and 0.2 respectively. This resulted in a 37% resolution of the amplitude of 800 km waves. For the surface data, the κ and γ were chosen to be 22,000 km² and 0.4 respectively. This resulted in a 27% resolution of the amplitude of 500 km waves. The reason for using this scheme is that resolution is achieved with one iteration and also small scale noise is suppressed (Barnes 1973). From the gridded datasets, charts were produced for each MCS case study with computed parameters such as Q-vector convergence, CAPE, equivalent potential temperature, and moisture convergence, and kinematic vertical motions. Observed data (T, Td,...) charts were also produced.

b. Analytical Techniques

After the satellite imagery loops were archived, storm motion, cell motion, and storm propagation vectors for each MCS were computed using programs written by myself, or by using pre-existing programs available on SLUATM or PC-McIDAS. The convective storm element was tracked as the centroid of the -52° C temperature area of the MCS in each loop because of the assumption that cold IR cloud tops are typically associated with deep

precipitating convective clouds. Cell motion was computed from hodograph data using the average wind or wind shear from 850-300 mb to represent the mean cloud layer wind of the MCS. Hodograph stations were selected based on their proximity to the storm complex and representativeness of the storm environment and storm propagation. Three or four stations were routinely chosen in order to form a triangle or a box around the MCS. This reduced the possibility that one unrepresentative station would represent the storm environment.

FORTTRAN programs were then used to compute the propagation vectors from the vector subtraction of storm velocity and cell velocity:

$$V_{\text{STORM}} - V_{\text{CELL}} = V_{\text{PROP}} \quad (1)$$

These vectors were then plotted using the CALPLOT software package which provided graphic display of the vectors influencing the storm propagation. Comparisons will be made between the propagation vectors computed using either the average wind vectors or the wind shear vectors in the 850-300 mb layer and the storm propagation, subjectively determined from the satellite imagery of each MCS, to see which exhibits the best correlation to the observed propagation. In an effort to characterize the environment which the MCS was propagating towards, a storm-relative (SR) inflow vector was computed as well, to see if a MCS propagates toward a certain type of environment (e.g., moist, unstable air, etc.). The SR inflow vector was computed as the vector difference

of the mean inflow vector and the storm motion vector, i.e.,

$$\mathbf{V}_{\text{MEAN}} - \mathbf{V}_{\text{STORM}} = \mathbf{V}_{\text{SR}} \quad (2)$$

The mean inflow vector was computed as the density-weighted mean wind from the surface to the level of free convection (LFC) at a rawinsonde site.

Case studies will be examined on an individual storm basis to note the factors influencing MCS propagation exhibited. Thirty-three MCS events will be examined from a database which was compiled from satellite imagery during the warm seasons (June-September) of 1990-1992. Three cases will be presented in detail to illustrate the different types of propagation usually exhibited by MCSs (forward, backward, and quasi-stationary). Our goal is to determine why certain storms propagate in a particular manner and if this propagation may be accurately predicted by forecasters in a operational environment using physical models of the synoptic and mesoscale environment.

4. DISCUSSION of RESULTS

a. Case Study 1, Forward Propagating MCS: 5 June 1991 1200 UTC

1. Description of the Event

Shortly after 0500 UTC 5 June 1991, a quasi-circular MCS developed in north-central Kansas. Over the next 15 hours the MCS dropped southward tracking nearly 800 km (500 miles) through Oklahoma. This case study will only focus on the portion of the track from eastern Kansas through northeast Oklahoma (0900-1400 UTC). This MCS, besides producing severe weather, was responsible for flash flooding in northeastern Oklahoma.

The initial convective development occurred during the early afternoon of 5 June along the central South Dakota/Nebraska border near a quasi-stationary front. This front was actually a "back door" cold front marking the western edge of cooler, drier air which had moved westward from the Ohio and Tennessee Valleys. By 0000 UTC 5 June, several small cloud clusters and a convective line (Bartels et al. 1984) were evident in the satellite imagery. By 0900 UTC a moderately sized quasi-circular MCS (also called a mini-MCC) had moved into eastern Kansas (see Fig. 8). Over the next five hours, this MCS grew in size. Although the five hours from 0900 to 1400 UTC does not meet the MCC duration criteria of six hours or more for a MCC (Maddox 1980), this MCS fulfilled the Maddox (1980) MCC criteria well before it reached northern Texas by 2000 UTC on this day. Its track during the 0900 to 1400 UTC period

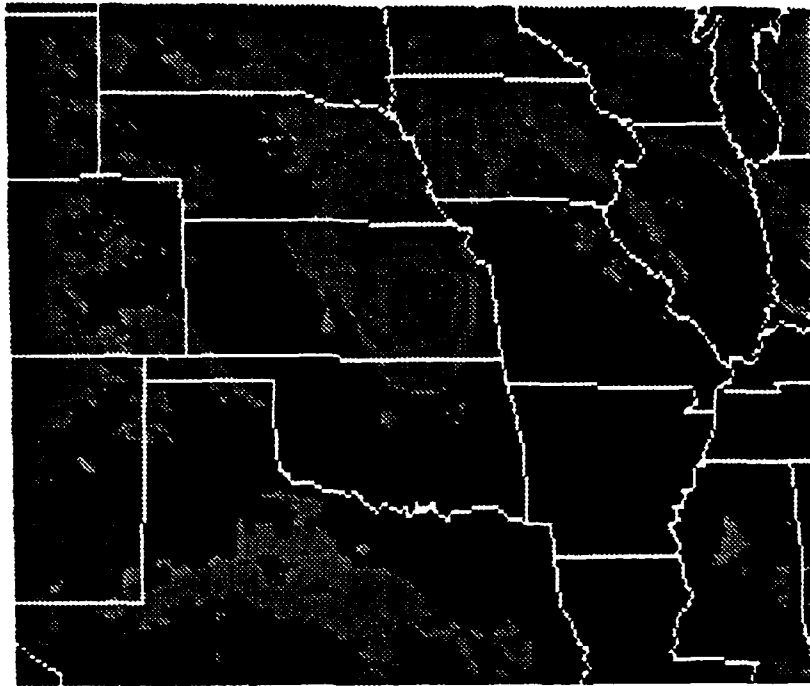


Figure 8. 09 UTC 5 June 1991 GOES satellite image using MB enhancement curve. Quasi-circular MCS located in eastern Kansas.

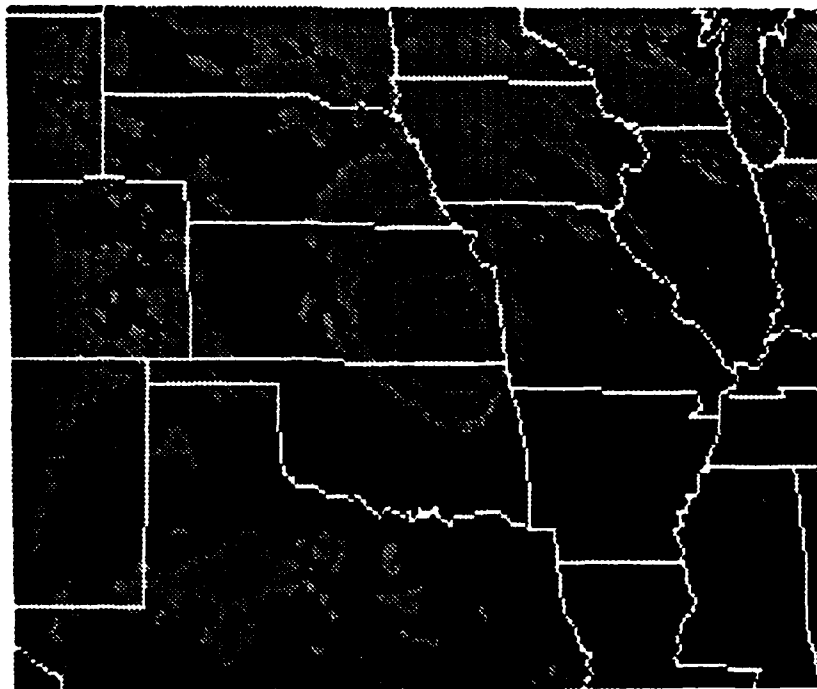


Figure 9. Same as in Fig. 8, except for 11 UTC.

was marked by a continuous forward propagation to the south-southeast. Figures 9, 10, and 11 depict the satellite images from 1100 UTC - 1400 UTC.

2) Synoptic and Mesoscale Conditions

Data available from 0000 UTC 5 June 1991 indicated healthy synoptic support at all levels for convection to occur across the central Plains. The surface analysis (Fig. 12) revealed a quasi-stationary front extending from west Tennessee across Missouri into central Nebraska. A temperature and dewpoint ridge were analyzed over east-central Kansas as a result of the flow from the south. Surface moisture convergence ($1.6 \text{ gm kg}^{-1}\text{-h}^{-1}$; not shown) was a maximum in central Nebraska and aligned with the frontal boundary. This showed that the front acted as a focusing mechanism for mesoscale lift. The orientation of the θ_e ridge paralleled the surface dewpoint ridge.

The upper air data from the same period revealed a stacked low at 500 and 300 mb over western South Dakota. Along with the 500 mb low was a vorticity maximum of $16 \times 10^{-5} \text{ s}^{-1}$ with a vorticity lobe extending southward into Oklahoma. This, though weak positive vorticity advection (PVA), was another source for lift. The fields over Nebraska and Kansas at 500 and 300 mb were generally west-southwest at 30 knots. Diffluence was evident at both levels with considerable diffluence noted across eastern Nebraska ahead of the shortwave. At 850 mb, two low level jets (LLJ) were analyzed (Fig. 13). The 850 mb temperature and dewpoint ridge (moist axis) were aligned quite well with the LLJ from Kansas to South Dakota. A second moisture axis located

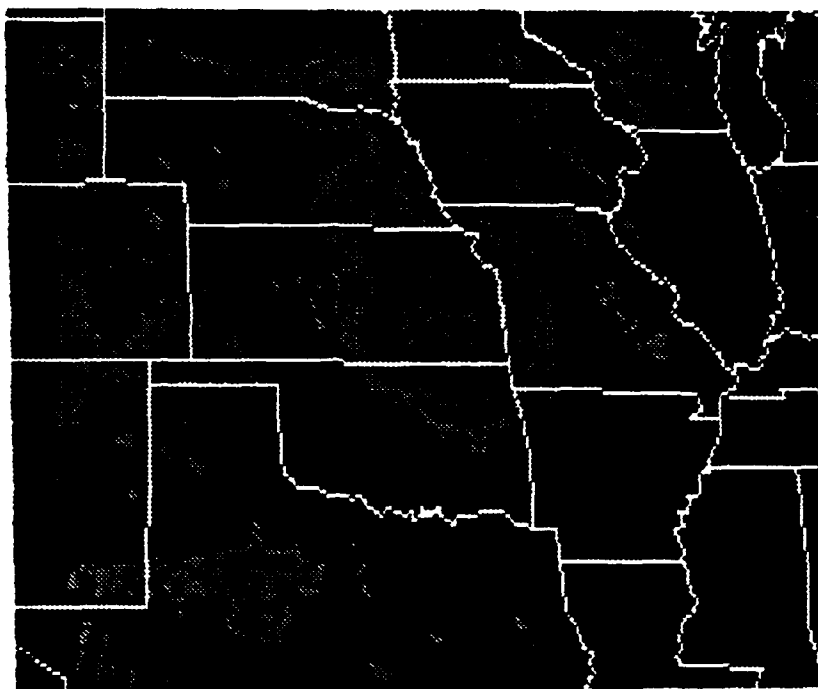


Figure 10. Same as in Fig. 8, except for 12 UTC.

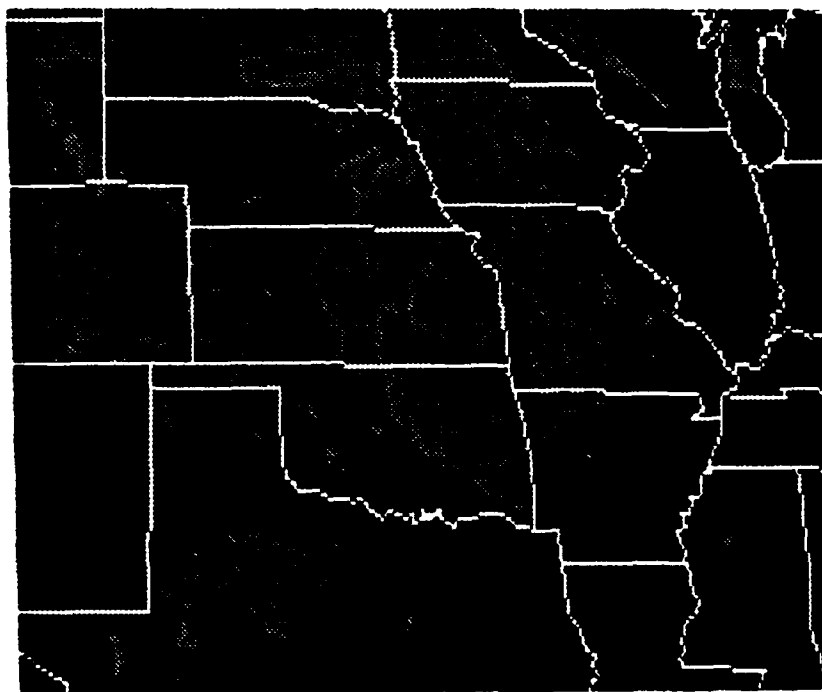


Figure 11. Same as in Fig. 8, except for 14 UTC.

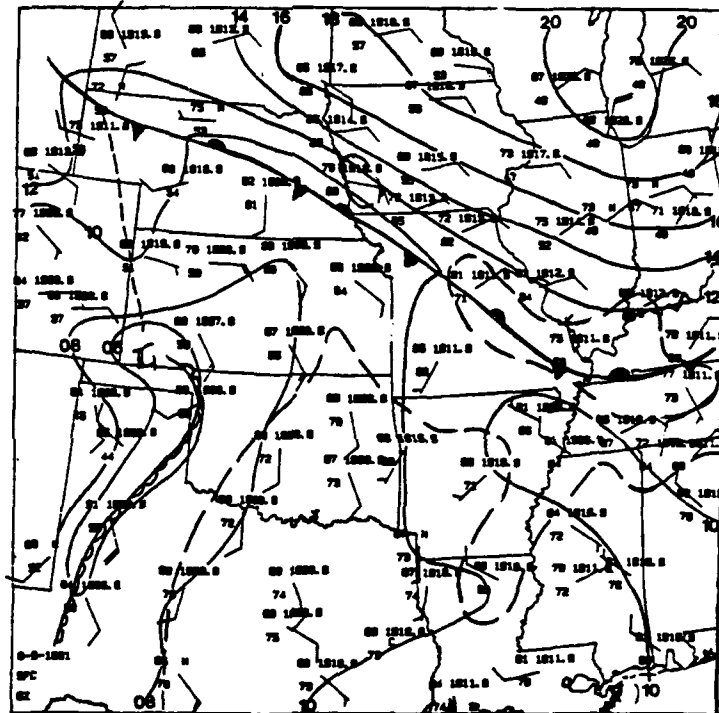


Figure 12. Surface weather map for 00 UTC 5 June 1991. Solid lines are isobars (in millibars) with the preceding 10 missing. Dashed line is 68° F isodrosotherm. Station model follows standard notation.

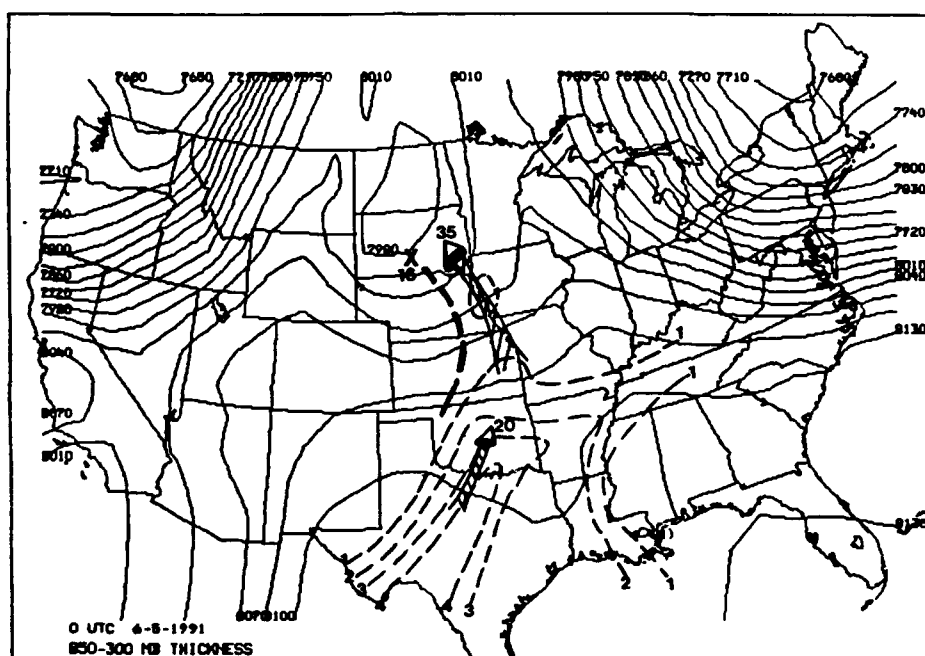


Figure 13. Composite chart for 00 UTC 5 June 1991. Solid lines are 850-300 mb thickness in gpm. Dashed lines are CAPE values in $10^3 \text{ Joules kg}^{-1}$. Bold X is absolute vorticity maximum with magnitude near X in 10^{-5} s^{-1} . Bold dashed lines are vorticity maximum axis. Arrow represents low-level jet axis with maximum wind value (in knots) at tip of arrow.

from the Big Bend area of Texas to southeast Oklahoma was coincident with a weaker LLJ in central Oklahoma. The 850 temperature advection was positive from east Texas north to North Dakota, indicating a warming trend in the lower levels with the northward transport of warm moist air from the south into the MCS region which may have provided additional mesoscale lift (Maddox and Doswell 1982).

The CAPE analysis (Fig. 13) for 0000 UTC revealed marginal CAPE values (less than 1000 J kg^{-1}) across Kansas/Nebraska, except for a maximum exceeding 1400 J kg^{-1} at Omaha, Nebraska (OMA). Across Oklahoma and Texas the CAPE was significantly higher ($> 3000 \text{ J kg}^{-1}$) indicating high instability in that area. The lifted index (LI) was -4 at OMA, while in southern Texas, the LI's were lower than -8. Overall, the areas of maximum instability were very closely related to the axes of low level moisture.

Shi and Scofield (1987) note that with sufficient lift, MCSs tend to develop within the 850 mb θ_e ridge axes and/or along maxima gradients. The 0000 UTC θ_e analysis diagnosed a ridge which extended northeast from southern Texas into Arkansas and then turned north into Nebraska was evident (Fig. 14).

By 1200 UTC, the convection was already well underway. The surface analysis (Fig. 15) revealed the changes that had happened since 0000 UTC. A convective outflow boundary was arcing from southwest Missouri across northern Oklahoma into central Kansas. The surface dewpoint ridge shifted west from its original position. At 500 mb, anticyclonic flow had developed due to height rises across the southern plains. It was evident on the 300 mb

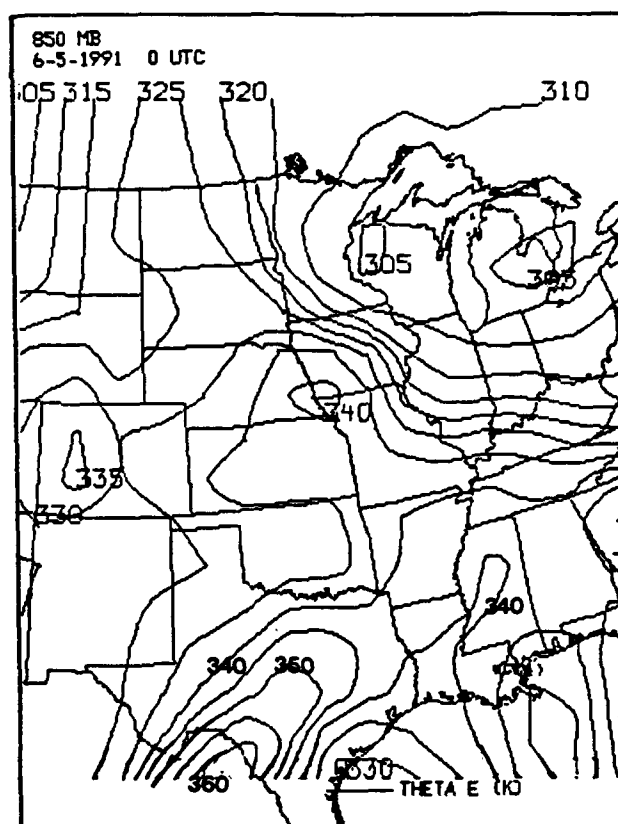


Figure 14. Equivalent potential temperature analysis for 850 mb for 00 UTC 5 June 1991 in degrees Kelvin.

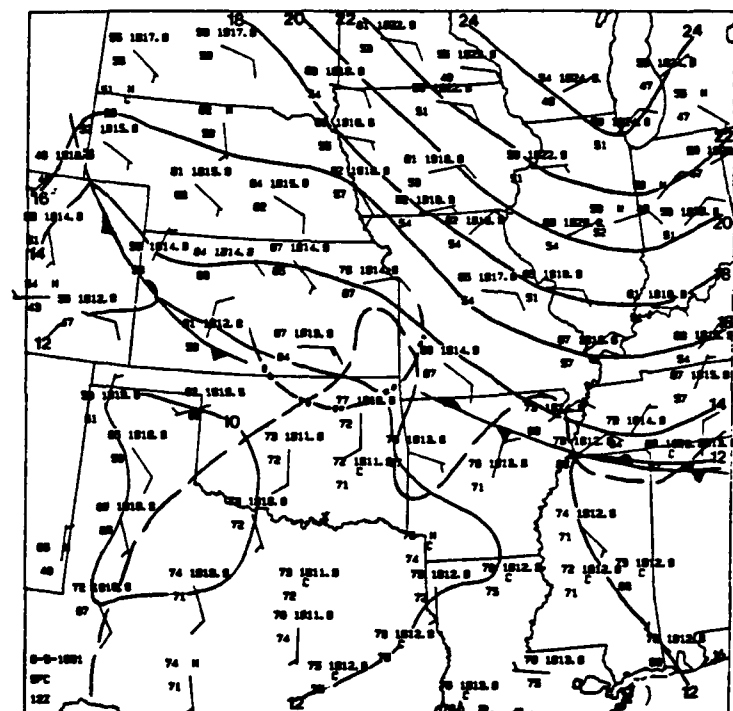


Figure 15. Same as in Fig. 12, except for 12 UTC.

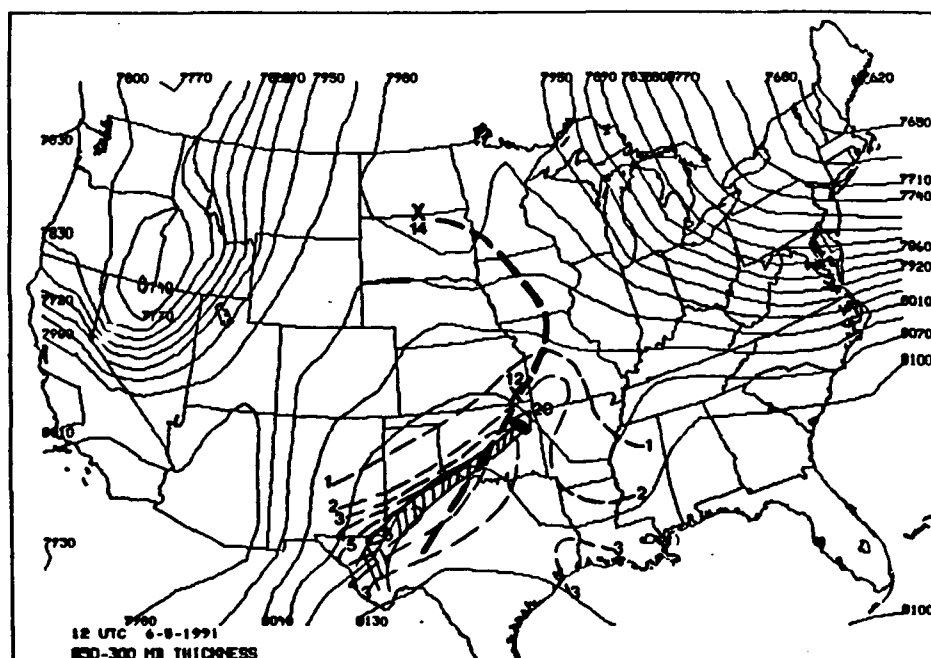


Figure 16. Same as in Fig. 13, except for 12 UTC.

analysis that diffluent flow over Kansas/Nebraska had developed since 00 UTC. At 850 mb, a LLJ (Fig. 16) was evident from the Texas Big Bend into central Oklahoma. Comparison to the 0000 UTC data indicate that the wind speeds had increased by 10 to 20 knots over this area. It is likely that the low level southerly flow increased overnight due to boundary layer stability changes (Blackadar 1957), however, the approach of the ULJ from Mexico may have also aided in the development of the southerly LLJ (Uccellini and Johnson 1979). The region from Texas up through eastern Nebraska at 850 mb was dominated by warm air advection, with a maximum over central Oklahoma. Strong moisture convergence was analyzed ahead of the MCS at 1200 UTC in the same area.

The CAPE values at 1200 UTC (Fig. 16) had changed dramatically overnight in west Texas with an area of significant instability ($> 3000 \text{ J kg}^{-1}$) from west Texas into eastern Oklahoma. This increase was more than likely caused by the increase in low level moisture and the strengthening of the low level southerly flow in west Texas. Note the westward shift of the 850 mb θ_e axis (Fig. 17).

3. Definition of Backward-Relative and Forward-Relative Propagating

MCSs

In cases where the magnitude of the mean tropospheric wind (or mean cell motion) is greater than the magnitude of the storm motion, the storm is said to exhibit backward-relative (B-REL) propagation. Essentially, the

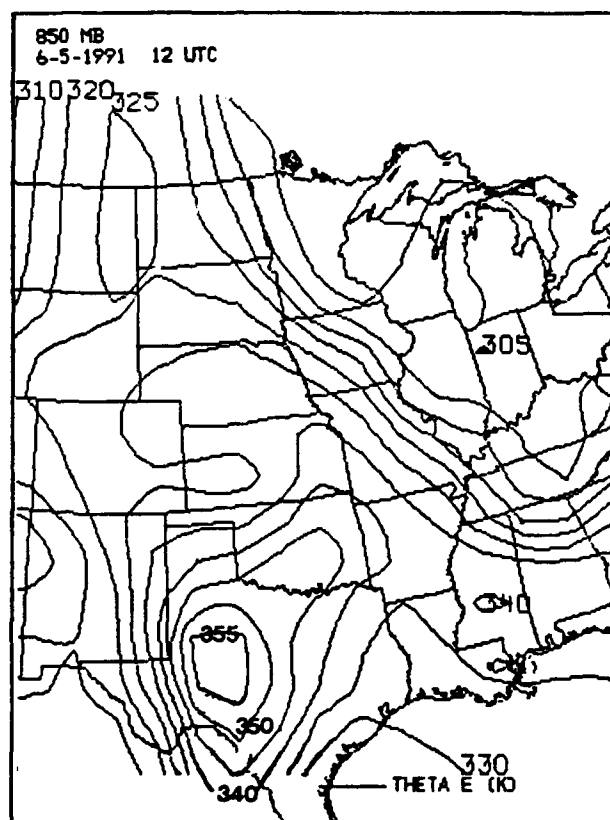


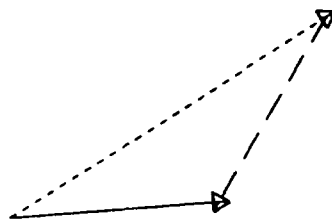
Figure 17. Same as in Fig. 14, except for 12 UTC.

environmental wind (which is representative of the cell motion) is moving faster than the computed storm motion (see Fig. 18). Although the Storm (MCS) is observed to move in generally a forward direction, in reality, it is moving **backward** relative to the mean flow. This is evident in the above figure where the propagation vector (V_{PROP}) has a component opposite to V_{CELL} .

In direct contrast to the above mentioned MCS is the Forward-Relative MCS. This type of propagation is exhibited when the magnitude of the mean tropospheric wind is less than the magnitude of the storm motion. (e.g., see Fig. 19). Shi and Scofield (1987) have also termed this type of MCS as a Fast-Forward propagating MCS.

4. Discussion of Propagation

Following MCS initiation, the storm propagation was from the northwest to the southeast (forward). This propagation appeared to be strongly influenced by the location of the source of high CAPE air from central Oklahoma. After 0900 UTC, satellite imagery showed the MCS located in southeastern Kansas. By 1200 UTC the MCS had moved almost due south into northeastern Oklahoma. An examination of the storm relative inflow vectors computed using Norman, OK (OUN); Little Rock, AR (LIT); and Monett, MO (UMN) at 1200 UTC show that the source region of the air flowing into the MCS at lower levels was still from the south (ahead of the MCS). The propagation during this time period (09-14 UTC) was best described by the 850-300 mb average wind vector (see Fig. 20 for the propagation vector plot). The observed storm motion



_____ = Storm Motion (265.1deg / 14.1 m/s)
 - - - - - = Cell Motion (237.5deg / 25.3 m/s)
 - . - . - = Propagation Vector (30.5 deg / 14.4 m/s)

Plotted using average wind 850-300mb

Using station: 72349
 72357
 72456

05-16-1990 00 UTC

Figure 18. Example of a propagation vector plot for a backward-relative propagating MCS.



_____ = Storm Motion (285.8deg / 15.2 m/s)
 - - - - - = Cell Motion (258.2deg / 6.8 m/s)
 - . - . - = Propagation Vector (304.8 deg / 9.7 m/s)

Plotted using average wind 850-300mb

Using station: 72235
 72340
 72357

09-09-1992 00 UTC

Figure 19. Same as in Fig. 18, except for forward-relative propagating MCS.



_____ = Storm Motion (329.5deg / 11.1 m/s)
 - - - - - = Cell Motion (270.4deg / 3.1 m/s)
 - - - - - = Propagation Vector (345.1 deg / 9.9 m/s)

Plotted using average wind 850-300mb

Using station: 72349
 72357
 72456

06-05-1991 12 UTC

Figure 20. Propagation vector plot for 5 June 1991 MCS.



_____ = Storm Motion (329.5deg / 11.1 m/s)
 - - - - - = Inflow Motion (349.7deg / 3.4 m/s)
 - - - - - = SR Inflow Vector (141.1 deg / 8.0 m/s)

Using station: 72340

06-05-1991 12 UTC

Figure 21. Storm-relative inflow vector plot for 5 June 1991 for Little Rock, AR.

was 329.5° at 11.1 m s^{-1} ; the cell motion was 270.4° at 3.1 m s^{-1} which resulted in a computed storm propagation vector of 345.1° at 9.9 m s^{-1} . This suggests a south-southeastward propagation which was observed in the imagery.

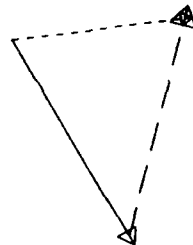
The storm-relative inflow vectors (Figs. 21, 22, and 23) were computed using Little Rock, AR (LIT); Norman, OK (OUN); and Monett, MO (UMN). They all indicate a southerly storm-relative inflow from a region of moist, unstable air and higher CAPE.

After 1400 UTC (1500 UTC image was unavailable) the MCS began a decided southwest propagation which appears to have been influenced by the repositioning of the CAPE and the 850 mb θ_e ridge axis. This demonstrates that within the same synoptic environment, a MCS can propagate in many different ways. The "signals" which seem to cause the MCS to begin propagating to the southwest were apparently received after 1400 UTC only when the magnitudes of the parameters became large enough to influence the MCS to develop away from its forward propagation track. However, through 1400 UTC, this MCS should be classified as a forward propagating MCS.

b. Case Study 2, Backward Propagating MCS: 11 September 1992 0000 UTC

1. Description of the Event

By 2100 UTC 10 September 1992, an almost circular MCS had met the MCC criteria described by Maddox (1980) having been in existence for six



_____ = Storm Motion (329.5deg / 11.1 m/s)
 - - - - - = Inflow Motion (263.0deg / 8.4 m/s)
 — — — = SR Inflow Vector (194.3 deg / 10.9 m/s)
 Using station: 72357
 06-05-1991 12 UTC

Figure 22. Same as in Fig. 21, except for Norman, OK.



_____ = Storm Motion (329.5deg / 11.1 m/s)
 - - - - - = Inflow Motion (226.7deg / 1.9 m/s)
 — — — = SR Inflow Vector (158.6 deg / 11.7 m/s)
 Using station: 72349
 06-05-1991 12 UTC

Figure 23. Same as in Fig. 21, except for Monett, MO.

hours by this time. From 2100 UTC 10 September 1992 to 0300 UTC 11 September 1992, the MCS tracked west-southwestward along an active east-west cold front. This MCS eventually dissipated and split into two distinct MCSs; each moving in opposite directions to the other. No Storm Data was available at this writing to verify precipitation totals or storm damage.

2. Synoptic and Mesoscale Conditions

Satellite imagery from 1200 UTC 10 September 1992 revealed a MCS already located in eastern Oklahoma along the same frontal boundary which later continued its movement into northern Texas at 00 UTC 11 September. Data from 1200 UTC 10 September indicated good synoptic support at all levels for MCS development in north Texas. The surface analysis for 1200 UTC (Fig. 24) revealed a cold front extending through central Arkansas across northern Texas and up into eastern New Mexico. High pressure behind the front helped turn the surface and 850 mb winds from out of the northeast. Upper air data from 1200 UTC revealed very light winds at all levels over Texas. The 500 mb vorticity field (Fig. 25) showed almost zero PVA to weak NVA extending into Texas. At 300 mb (Fig. 26), the jet core was well north of Texas in eastern Wisconsin. At 850 mb (Fig. 27), strong moisture convergence and a θ_e ridge axis were located over central Texas. On the 1200 UTC composite chart, thickness diffluence is evident in the 850-300 mb thickness field. Warm air advection at this level at 1200 UTC covered the northern half of Texas.

CAPE was used to evaluate environmental stability. The composite

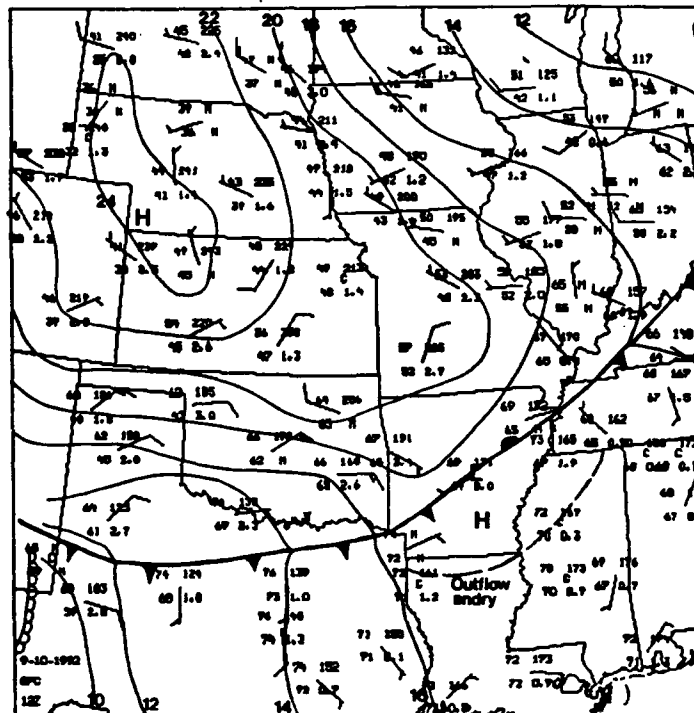


Figure 24. Surface weather map for 12 UTC 10 September 1992. Solid lines are isobars (in millibars) with the preceding 10 missing. Scalloped lines is dryline. Station model follows standard notation.

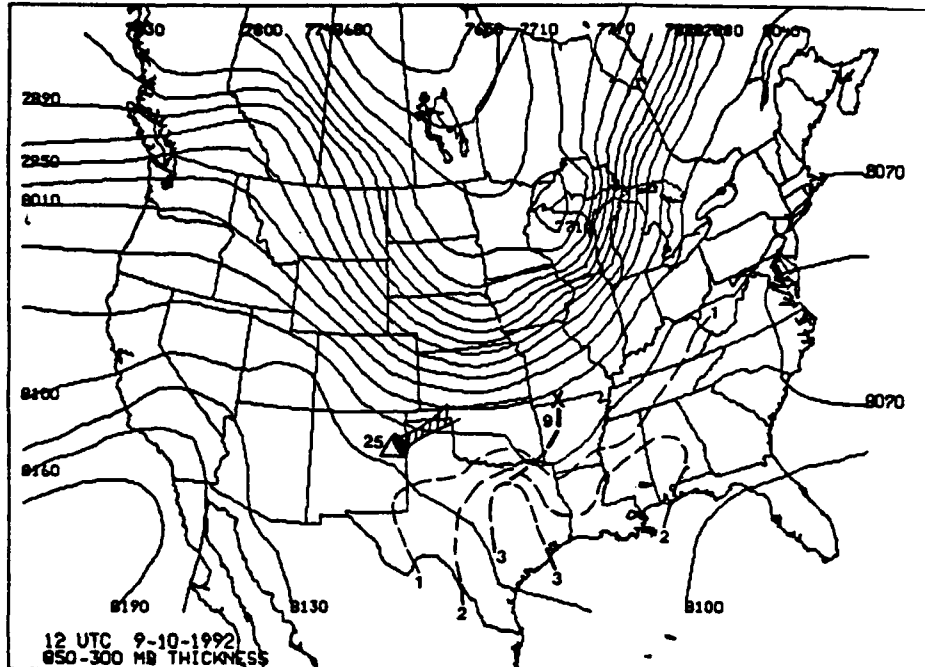


Figure 25. Composite chart for 12 UTC 10 September 1992. Solid lines are 850-300 mb thickness in gpm. Dashed lines are CAPE values in $10^3 \text{ Joules kg}^{-1}$. Bold X is absolute vorticity maximum with magnitude noted near X in 10^{-5} s^{-1} . Bold dashed line is vorticity maximum axis. Arrow represents low-level jet axis with maximum wind value (in knots) at tip of arrow.

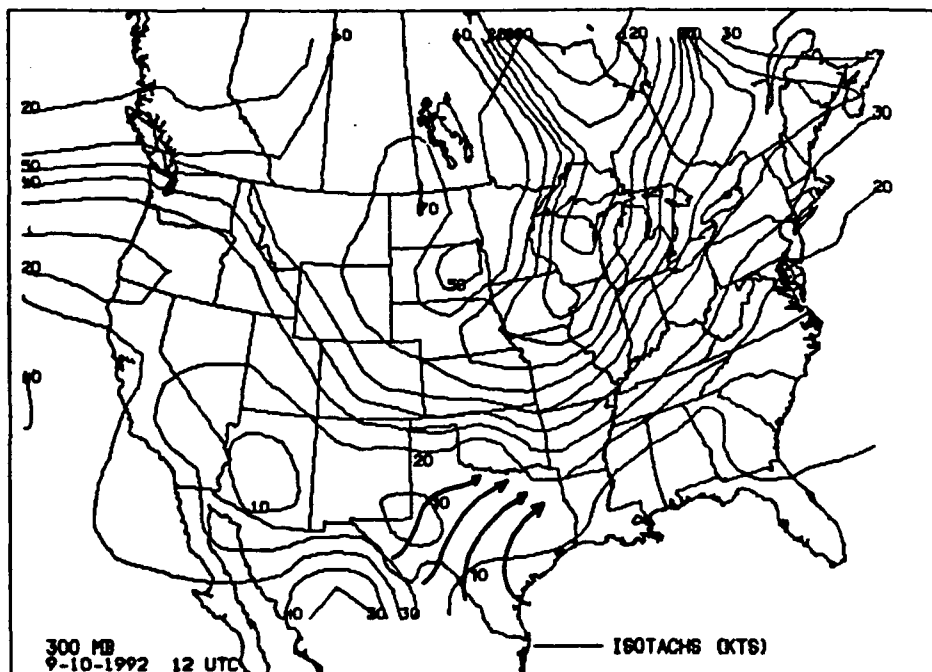


Figure 26. 300 mb isotachs (in knots) for 12 UTC 10 September 1992. Arrows indicate direction of wind flow.

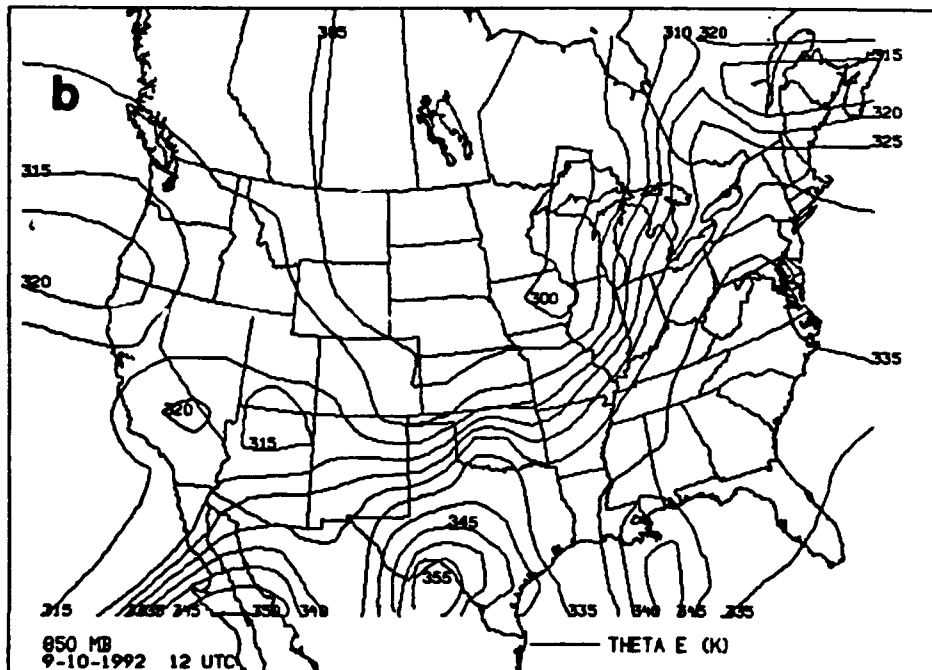
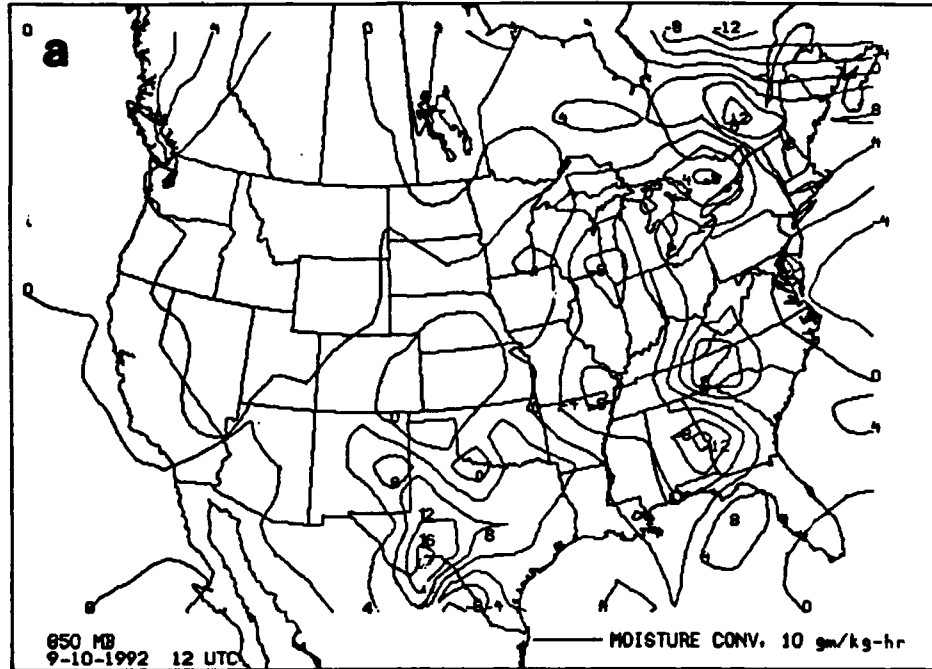


Figure 27. (a) 850 mb moisture convergence for 12 UTC 10 September 1992. Values $\times 10 \text{ gm kg}^{-1}\text{-hr}^{-1}$ (b) 850 mb θ_e for 12 UTC. Values in degrees Kelvin.

figure for 1200 UTC (Fig. 25) reveals strong CAPE values (more than 3000 J kg⁻¹) in central-eastern Texas. Lifted indices in this area were -4 to -6.

By 2100 UTC 10 September 1992, the MCS had moved into this very unstable area (Fig. 28). The winds at the upper levels remained very light over Texas, except at 850 mb. At the surface, the cold front nosed into central Texas by 0000 UTC 11 September 1992 (Fig. 29). The surface dewpoint analysis at 0000 UTC (Fig. 30) indicated an area of dewpoint pooling in western Texas where dewpoint values increased four to six degrees and had shifted to the west. Along with this westward shift of the 64° isodrosotherm, the surface θ_e ridge axis also shifted west into extreme western Texas (Fig. 31). The 850 mb wind maximum, shown in Fig. 33, indicated a 25 knot wind max (LLJ) originating from the anticyclonic flow from the high pressure trailing the front. This may help, in part, to explain the motion of the MCS toward the southwest. There was also a decided westward shift of the 850 mb θ_e ridge axis similar to the surface axis (Fig 32). The convective stability analysis for Del Rio, Texas revealed an almost 25° drop in θ_e from the surface to 650 mb; an indication of the degree of instability of the airmass ahead of the MCS. The upper air data from 0000 UTC revealed continued light and variable winds at all levels. At 300 mb, at 0000 UTC, the winds had increased to only 20 knots in 12 hours. As seen in the 00 UTC composite chart, Fig. 33, at 500 mb, weak PVA associated with the tail end of a $21 \times 10^5 \text{ s}^{-1}$ vorticity maxima near Hudson Bay was moving southeast through central Texas at this time.

The CAPE values at 0000 UTC (Fig. 33) had changed with the area of

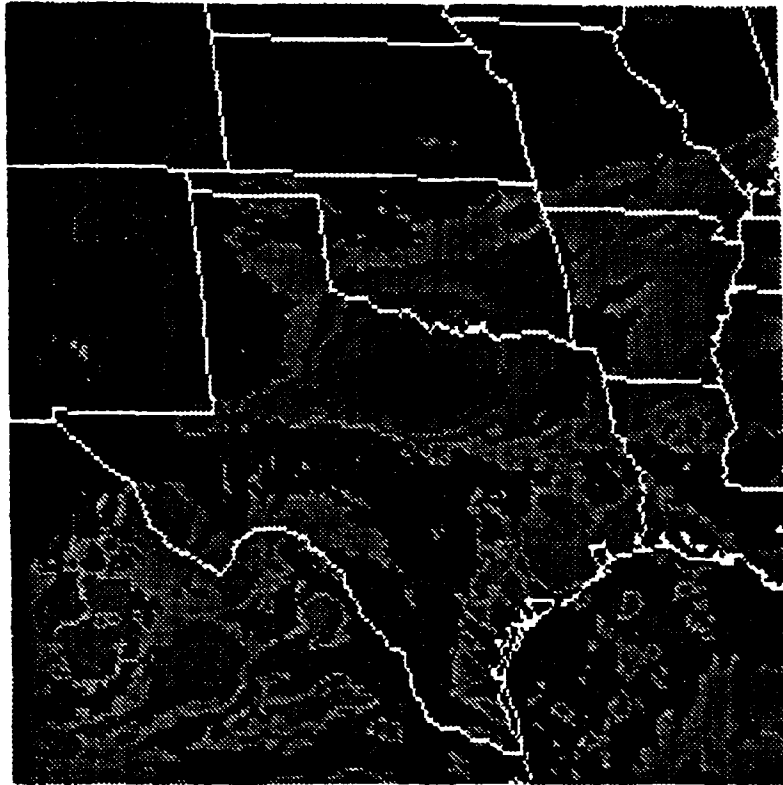


Figure 28. Satellite image for 21 UTC 10 September 1992.

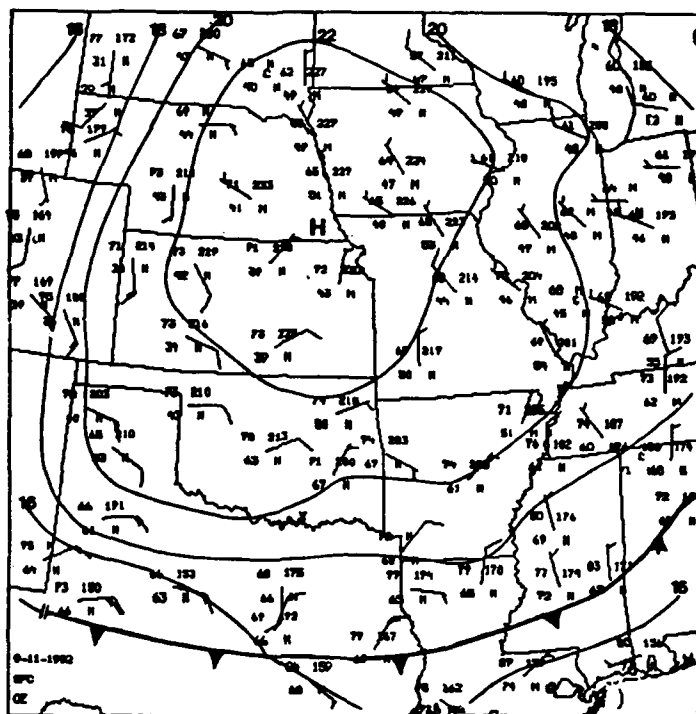


Figure 29. Same as in Fig. 24, except for 00 UTC 11 September 1992.

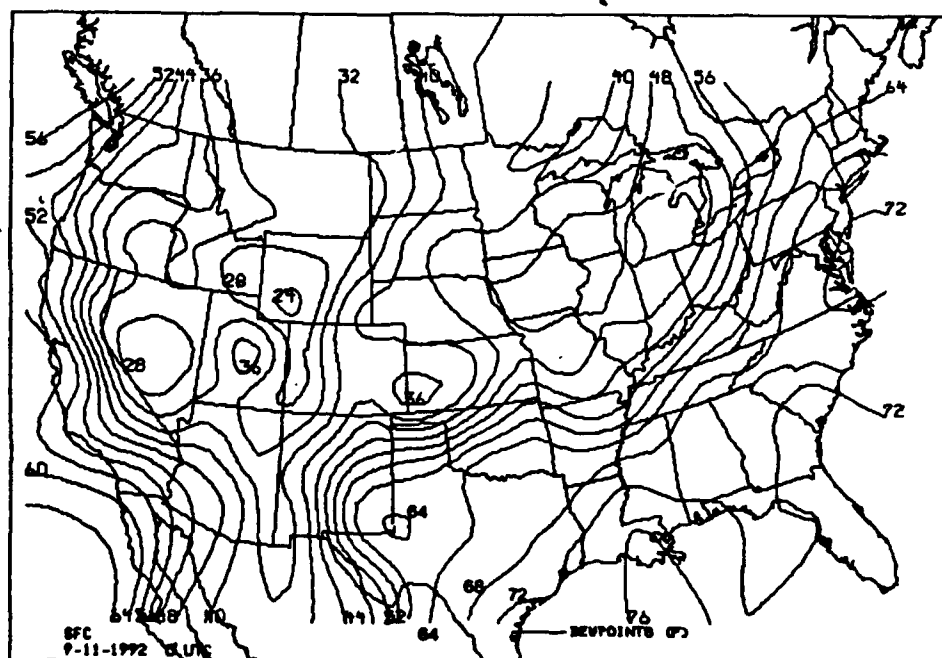


Figure 30. Surface dewpoints for 00 UTC 11 September 1992 in degrees F.

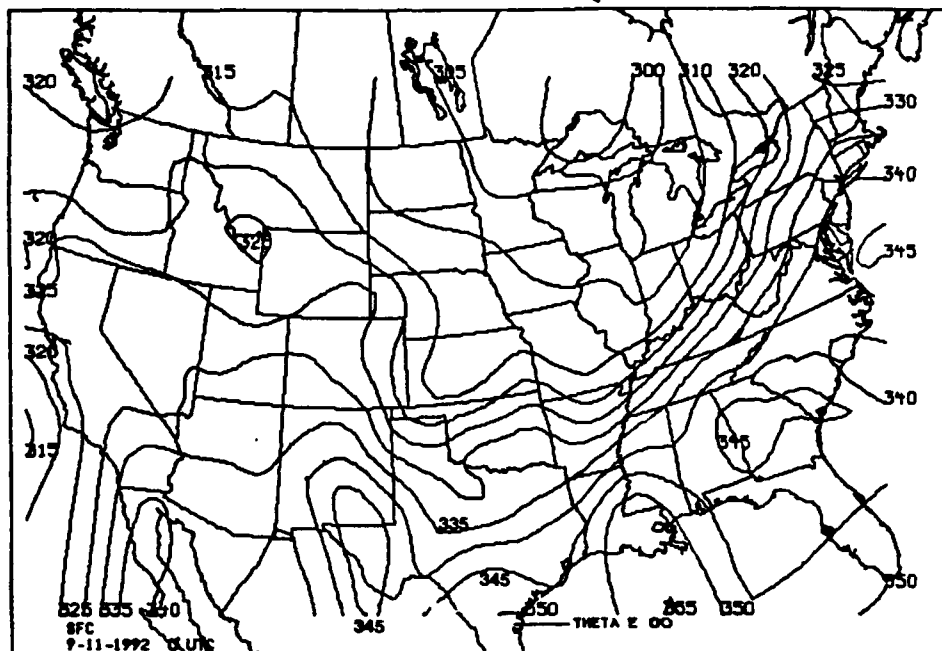


Figure 31. Surface θ_e for 00 UTC 11 September 1992 in degrees Kelvin.

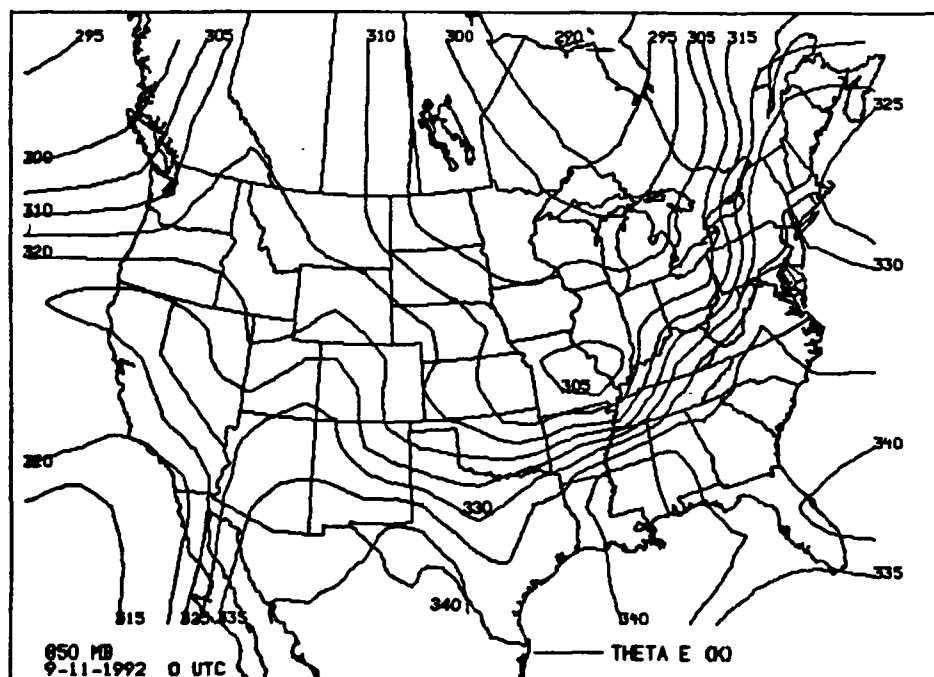
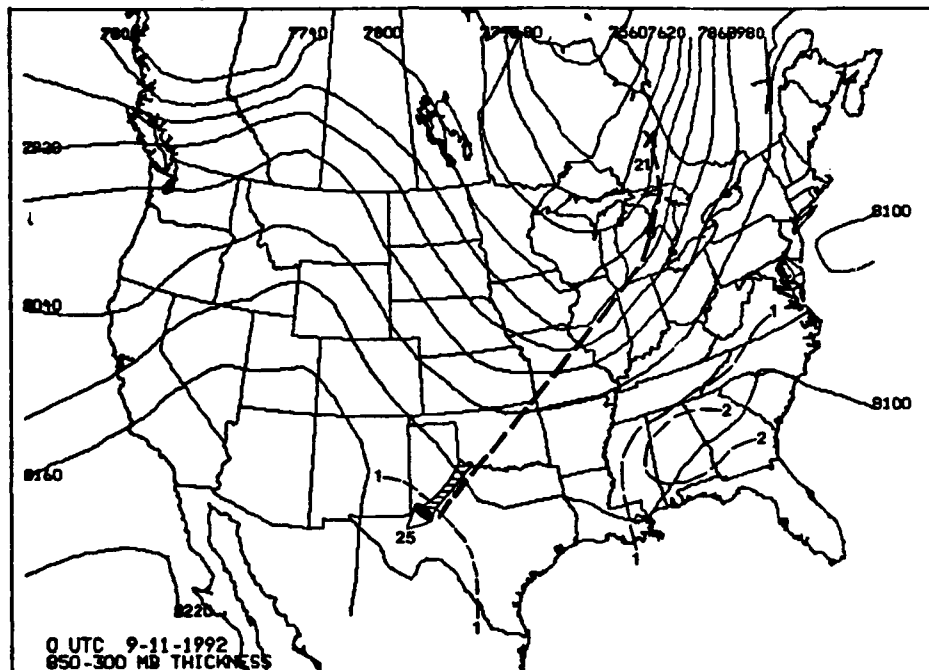


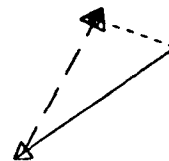
Figure 32. Same as in Fig. 27b, except for 00 UTC 11 September 1992.



moderate instability relocating in the Del Rio, TX area where a value of 1900 J kg⁻¹ was analyzed. More than likely, the cause for this new CAPE maximum was the shift of the θ_e ridge axis and the westward shift of moisture at the surface. With the influence of the cold front bringing in more stable air, LIs dropped to -2 to -4 in the area.

3. Discussion of Propagation

The 850 mb LLJ analyzed at 0000 UTC 11 September appears to have contributed very little to enhance the low level moisture transport in this case. However, it may have served the purpose of providing a low level steering flow to guide the MCS. The direction or propagation of this MCS may have also been influenced by the location and orientation of the surface frontal zone. With those facts, and the western location of the surface moisture (dewpoints), surface and 850 mb θ_e ridge axes, and the CAPE maximum, it is evident that the rich source of "fuel" for MCS sustenance was west (ahead) of the MCS in this case. By examining the computed storm-relative inflow vectors from Del Rio, TX (DRT); Midland, TX (MAF); and El Paso, TX (ELP) (Figs. 34, 35, and 36), it is clear that the region west of the MCS is the favored region for the MCS to propagate toward. Using the averaged 0000 UTC 850-300 mb shear for Amarillo, TX (AMA); Del Rio, TX (DRT); and El Paso, TX (ELP), and an observed storm motion of 55.5° at 12.5 m s⁻¹, a storm propagation vector of 83.4° at 12.8 m s⁻¹ was calculated (Fig. 37) which provides a better correlation to the observed storm propagation than the average wind 850-300 mb (using the



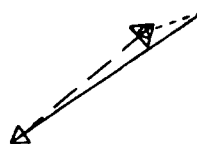
_____ = Storm Motion (55.5 deg / 12.5 m/s)
 ----- = Inflow Motion (110.1deg / 5.7 m/s)
 - - - - = SR Inflow Vector (208.7 deg / 10.3 m/s)
 Using station: 72261
 09-11-1992 00 UTC

Figure 34. Storm-relative inflow vector plot for 11 September 1992 for Del Rio, TX.



_____ = Storm Motion (55.5 deg / 12.5 m/s)
 ----- = Inflow Motion (76.6 deg / 4.1 m/s)
 - - - - = SR Inflow Vector (225.8 deg / 8.8 m/s)
 Using station: 72265
 09-11-1992 00 UTC

Figure 35. Same as in Fig. 34, except for Midland, TX.



_____ = Storm Motion (55.5 deg / 12.5 m/s)
 - - - - - = Inflow Motion (70.5 deg / 3.6 m/s)
 - . - . - = SR Inflow Vector (229.6 deg / 9.1 m/s)
 Using station: 72270
 09-11-1992 00 UTC

Figure 36. Same as in Fig. 34, except for El Paso, TX.



_____ = Storm Motion (55.5 deg / 12.5 m/s)
 - - - - - = Cell Motion (336.7 deg / 6.1 m/s)
 - . - . - = Propagation Vector (83.4 deg / 12.8 m/s)
 Plotted using wind shear 850-300mb
 Using station: 72261
 72270
 72363
 09-11-1992 00 UTC

Figure 37. Propagation vector plot for 11 September 1992 MCS.

same stations).

An interesting feature of this MCS was the storm splitting that occurred shortly before the 02 UTC 11 September 1992 satellite image (Fig. 38). The storm split into two separate cloud clusters with one in western Texas and the other in eastern Texas. After splitting, each cluster tracked closely along the 850 mb θ_e ridge axis in its area.

c. Case Study 3, Quasi-Stationary Propagating MCS: 15 June 1992 0000 UTC

1. Description of the Event

During the late afternoon of 15 June 1992, strong convection broke out along an east-west stationary front draped across northern Kansas and central Missouri, close to an impressive dry line extending from northwest-central Kansas into the Big Bend of Texas. At 2100 UTC 15 June 1992, a small convective cloud with an anvil blowoff was evident in the satellite imagery. By 2200 UTC, the complex had more than tripled in coverage on the imagery and exhibited an almost stationary nature. During the early evening and evening hours, this MCS grew to MCC proportions, and exhibited a quasi-stationary propagation pattern. The MCS eventually dissipated well after 0800 UTC 16 June 1992. Storm Data for this MCS were unavailable at this writing to evaluate storm damage.

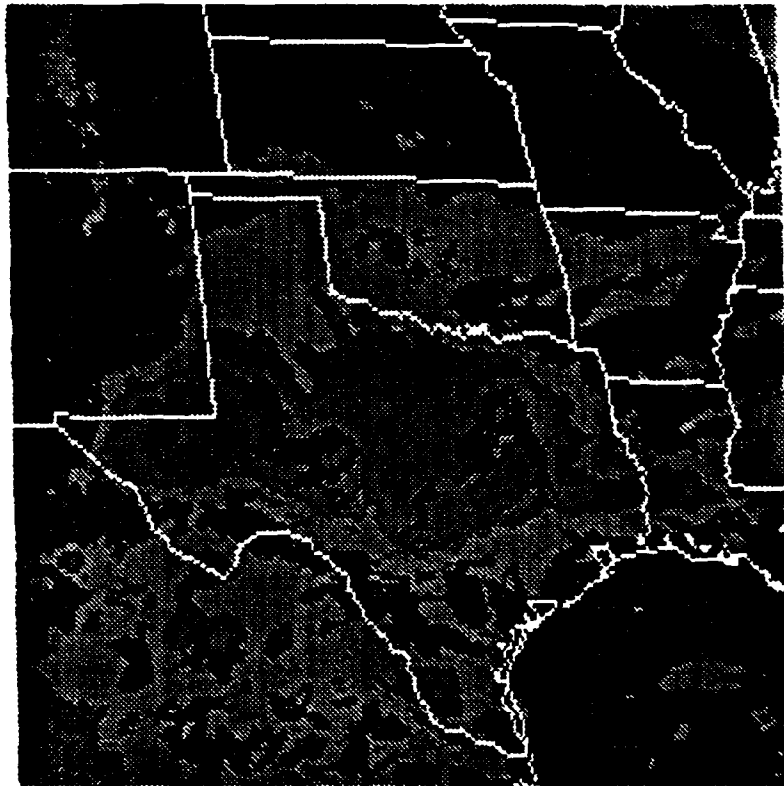


Figure 38. Satellite image for 02 UTC 11 September 1992.

2. Synoptic and Mesoscale Conditions

Data available from 0000 UTC 16 June 1992 indicated very favorable conditions for MCS development across eastern Kansas and Nebraska. Those features characterized in the MCC genesis region (Maddox 1983) and present across Kansas and Nebraska included: an east-west frontal zone, an 850 mb jet (LLJ), significant warm air advection, very unstable air within the south and east portion of this area, and veering of the winds with height from the surface up to 300 mb.

The surface analysis at 2100 UTC (Fig. 39) indicated an east-west stationary front, a 1000 mb closed-low over northwest Kansas, and a strong dryline stretching from western Kansas through Oklahoma and into southwest Texas. The surface wind field details the strong flow from the south. The air mass across the Nebraska/Kansas/Oklahoma region was characterized by a large area of surface dewpoints exceeding 70° F in some locations. At 0000 UTC temperatures south of the stationary boundary and east of the dry line were in the 80°s F (Fig. 40). The surface moisture divergence field, Fig. 41 was a - 3.2 g kg⁻¹-hr⁻¹ convergence bullseye over north-central Kansas. At 500 and 200 mb, diffluent flow was quite evident. At 500 mb west-southwest flow dominated the pattern from an upper level low in the western United States. A vigorous short wave passed through this region before 0000 UTC. The composite chart for 0000 UTC (Fig. 42) displays almost no positive vorticity advection at 500 mb. The position and strength of the 850 mb LLJ (Fig. 42) and the 850 mb θ_e ridge axis (Fig. 43) indicate that highly unstable air was

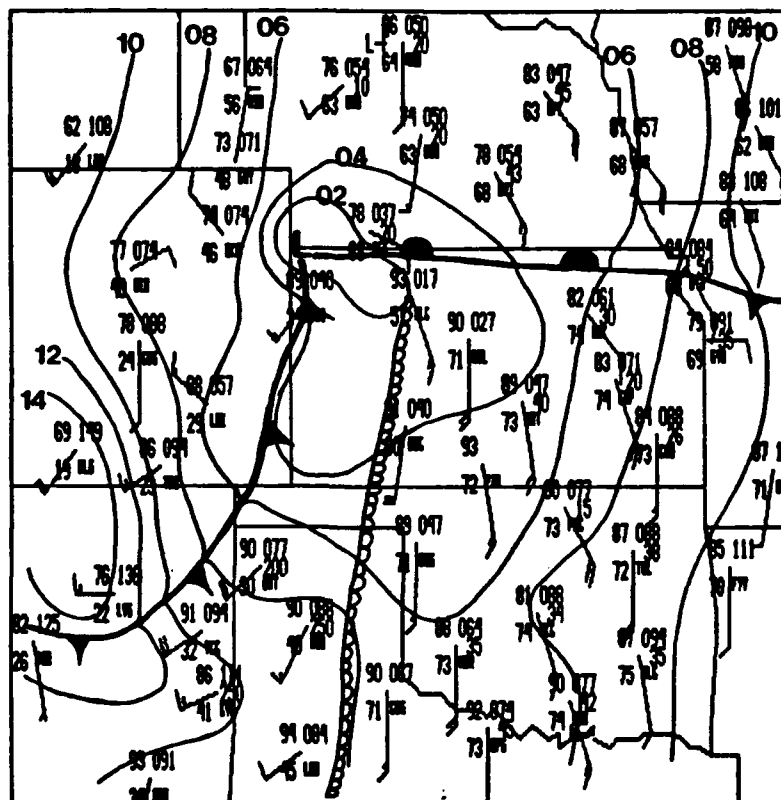


Figure 39. Surface weather map for 21 UTC 15 June 1992. Solid lines are isobars (in millibars) with the preceding 10 missing. Scalloped line is dryline. Station model follows standard notation.

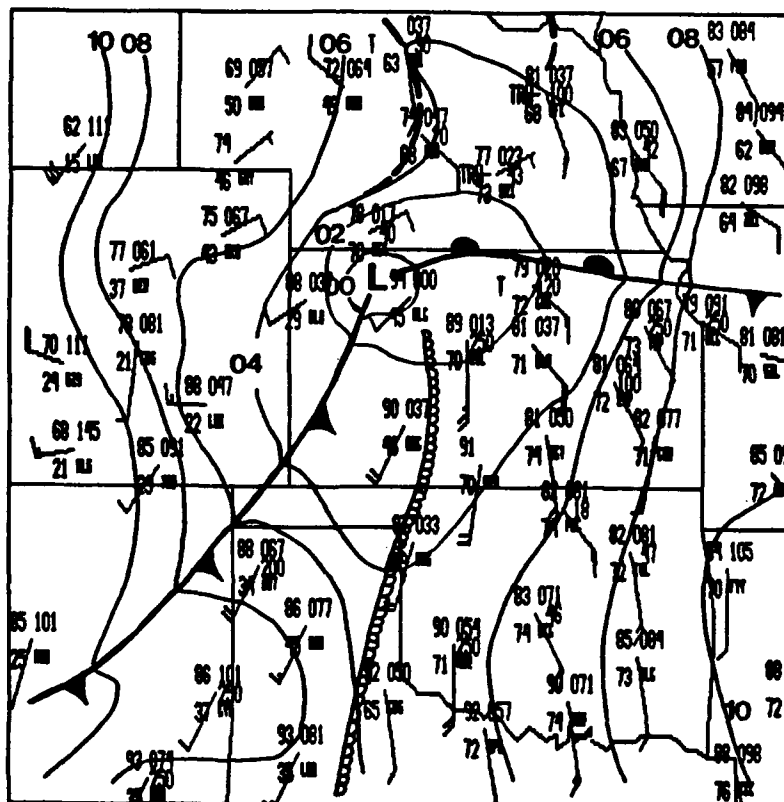


Figure 40. Same as in Fig. 39, except for 00 UTC 16 June 1992.

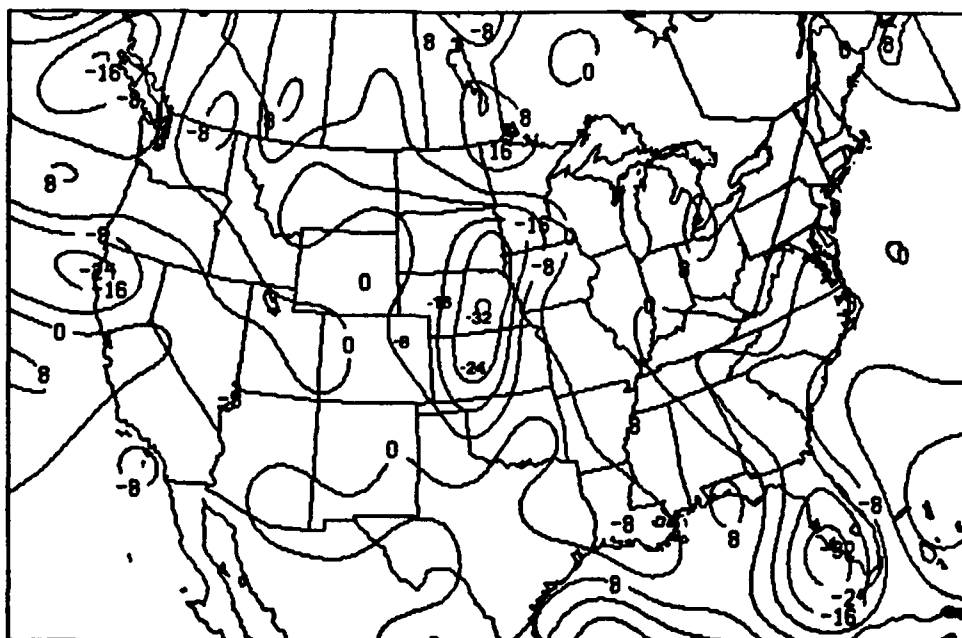


Figure 41. Surface moisture divergence for 00 UTC 16 June 1992. Minus signs are moisture convergence in $\text{gm kg}^{-1}\text{-hr}^{-1} \times 10$.

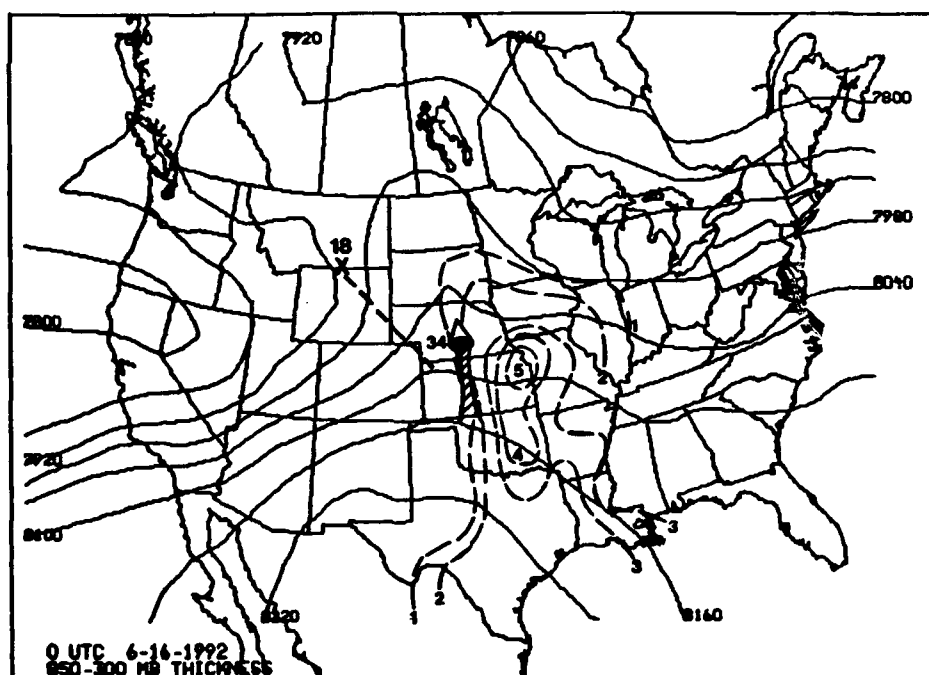


Figure 42. Composite chart for 00 UTC 16 June 1992. Solid lines are 850-300 mb thickness in gpm. Dashed lines are CAPE values in $10^3 \text{ Joules kg}^{-1}$. Bold X is absolute vorticity maximum with magnitude near X in 10^5 s^{-1} . Bold dashed line is vorticity maximum axis. Arrow represents low-level jet axis with maximum wind value (in knots) at tip of arrow.

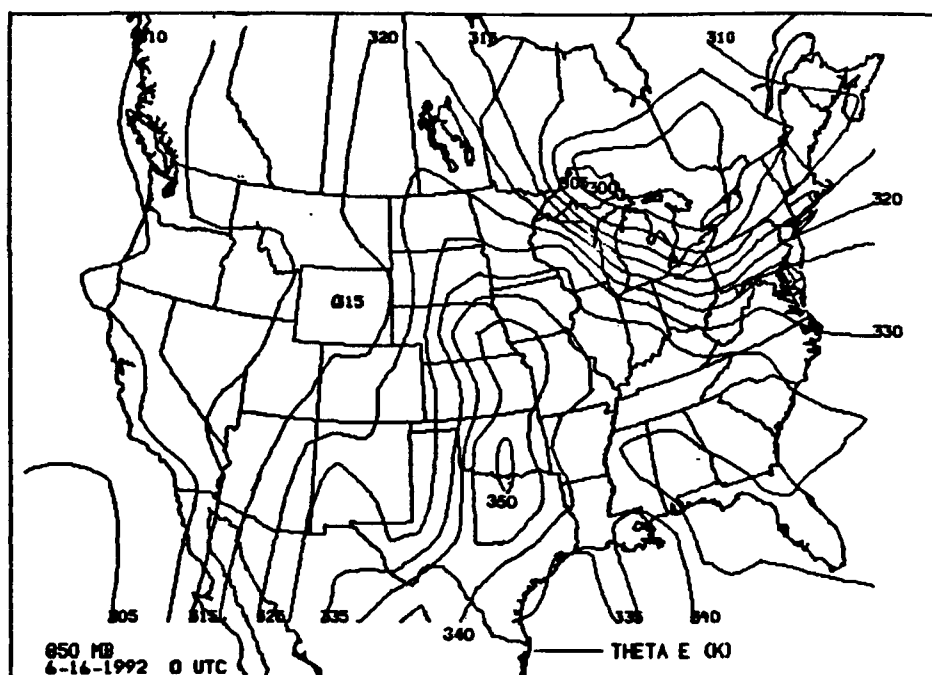


Figure 43. 850 mb θ_e for 00 UTC 16 June 1992 in degrees Kelvin.

being transported to the approximate MCS location.

The convective stability analysis (Fig. 44) (θ_e cross-section) over Topeka, KS at 0000 UTC on 16 June shows an almost 65° drop of θ_e from 800 mb to 970 mb. The skew-T sounding from Topeka at the same time (Fig. 45), shows the classic "Loaded Gun" sounding (Fawbush and Miller 1953) associated with tornadoes in the Plains region. The CAPE values for 0000 UTC were very impressive across eastern Kansas with values exceeding 5500 J kg^{-1} at Topeka as seen in Fig. 42. Lifted indices were in the -6 to -10 range. The 850 mb 0000 UTC θ_e values showed a strong ridge axis from south Texas north through central North Dakota.

3. Discussion of Propagation

In most instances, MCSs are observed to propagate with a deliberate forward or backward component, with respect to the environment. However, in some cases, a MCS may exhibit little or no propagation in any specific direction and be classified as a quasi-stationary (Q-S) propagating MCS. This MCS case study is an example of a Q-S MCS.

Following MCS initiation at approximately 2100 UTC 15 June, very little in the way of eastward movement of the MCS was noted through 0300 UTC 16 June on satellite imagery (Figs. 46-49). Weaver (1979) examined how severe thunderstorms may become anchored to intense boundary layer convergence zones. It appears that this MCS was "anchored" in some fashion to a boundary layer convergence zone. This may have been possibly due to the

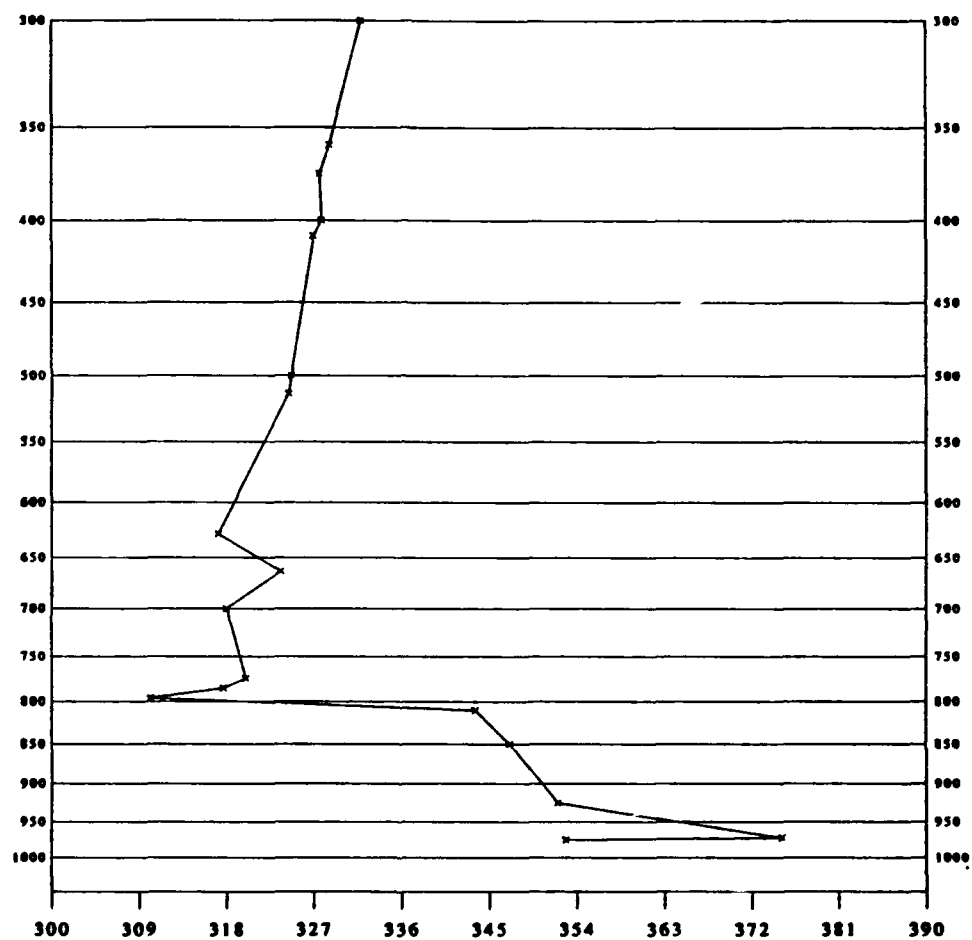


Figure 44. Convective stability analysis for Topeka, KS 00 UTC 16 June 1992. Values on y-axis are pressures in millibars and x-axis are θ_e in degrees Kelvin.

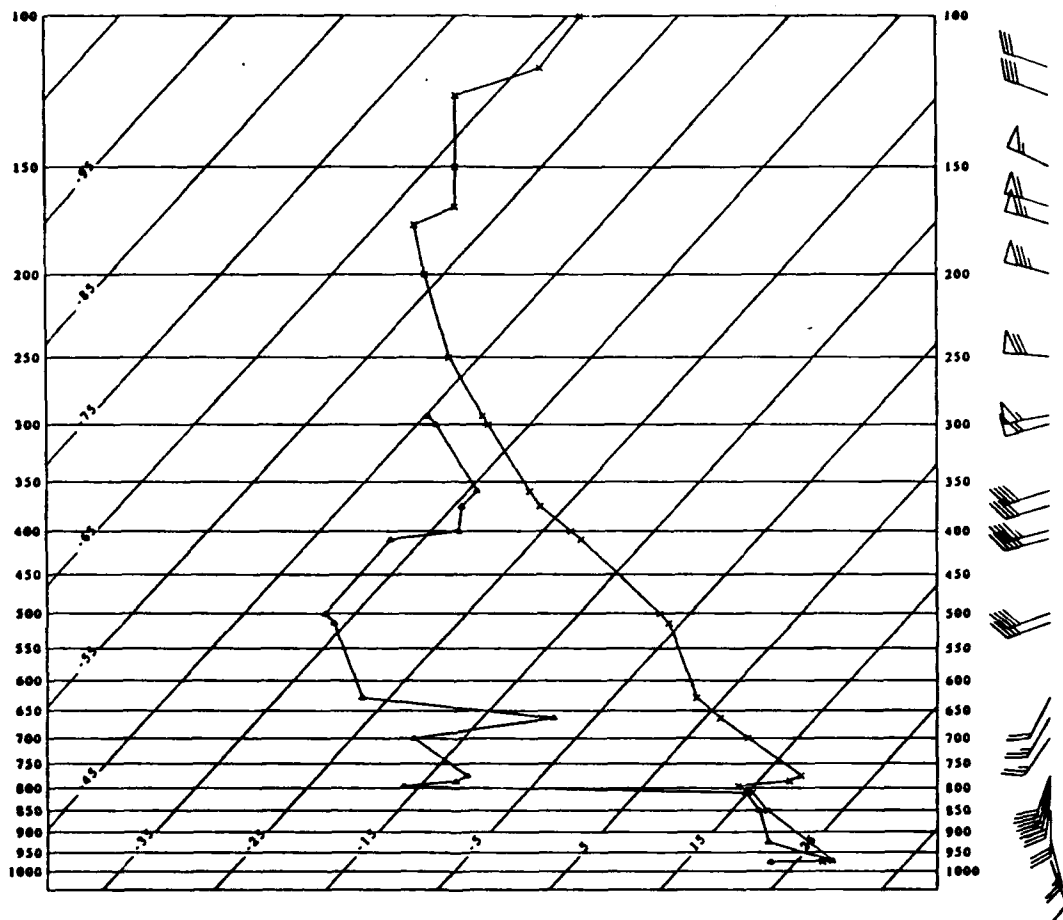


Figure 45. Skew-T Log P diagram for Topeka, KS 00 UTC 16 June 1992.

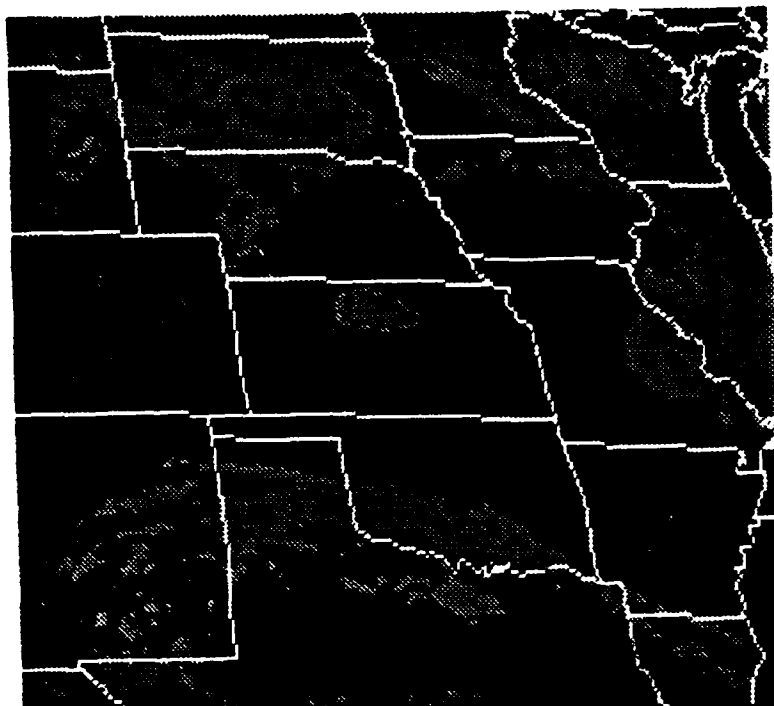


Figure 46. Satellite image for 21 UTC 15 June 1992.

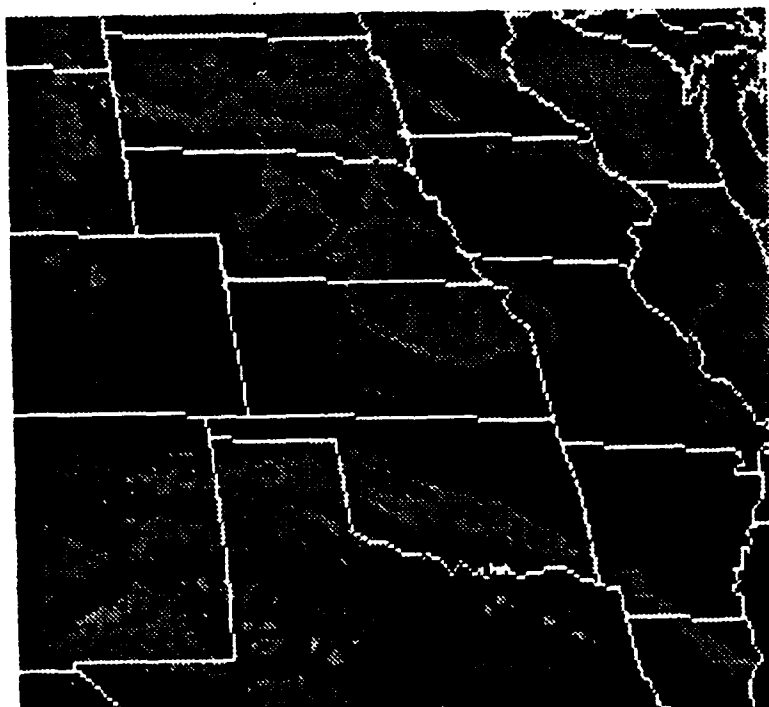


Figure 47. Satellite image for 23 UTC 15 June 1992.

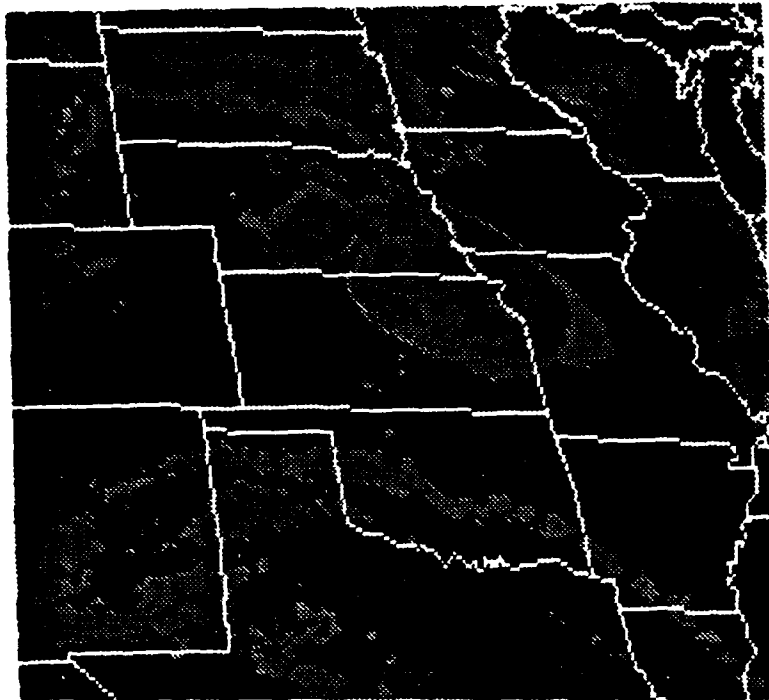


Figure 48. Same as in Fig. 47, except for 00 UTC 16 June 1992.

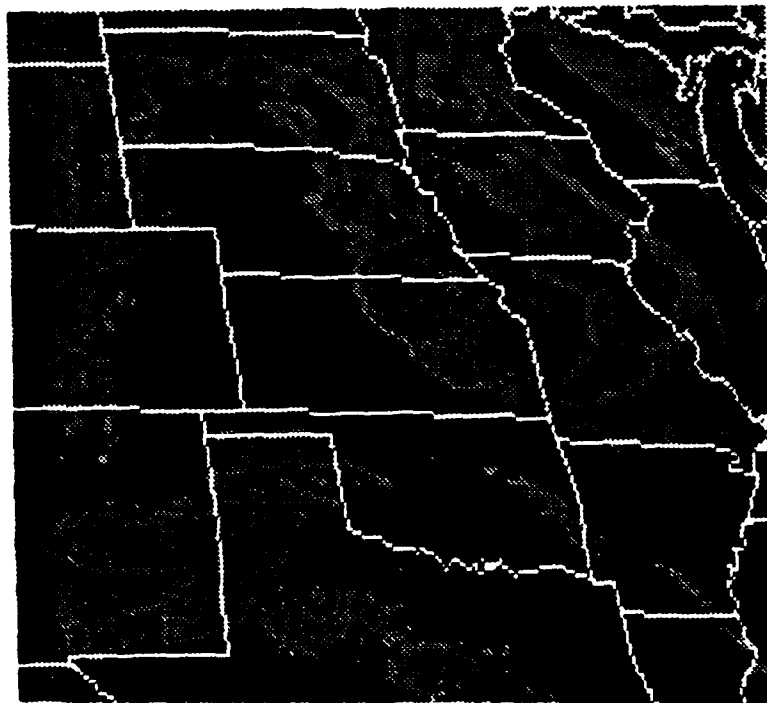
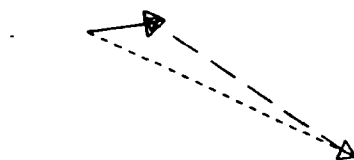


Figure 49. Same as in Fig. 47, except for 03 UTC 16 June 1992.

position and/or magnitude of parameters or features common to the boundary layer.

The presence of the strong surface moisture convergence at 0000 UTC (Fig. 41) across central Kansas and Nebraska underlie the existence of a possible boundary layer convergence zone. In Fig. 43, the 850 mb θ_e ridge axis at 0000 UTC was oriented north-south and just to the east of the surface moisture convergence maximum. These factors, in addition to the positions of the surface front, extremely high CAPE ($> 5000 \text{ J kg}^{-1}$), a dryline, and the LLJ, seem to have aided greatly in enhancing the Q-S propagation exhibited by this MCS.

In this case, the propagation vector apparently offset the mean cloud-layer wind vector by being oriented almost anti-parallel to it (Fig. 50). Storm-relative inflow vectors (Figs. 51-53) computed using Topeka, KS; Dodge City, KS; and Norman, OK all indicate a southerly directed storm-relative inflow vector. This is significant because the source region of these vectors was an area with: maximum 850 mb θ_e temperature, warm air advection, and CAPE values exceeding 4000 J kg^{-1} . All of these act as sources of instability "fuel" for the MCS. Evidently, the combination of these storm-relative inflow vectors, the propagation vector, and the synoptic conditions were properly oriented in position and strength to inhibit the MCS from propagating forward or backward. Instead, a complicated combination of the two resulted. In addition, by 1200 UTC 16 June, the 850 mb θ_e ridge axis (Fig. 54) had moved only slightly eastward into eastern Kansas indicating that the unstable air had not moved too



_____ = Storm Motion (262.3deg/6.3 m/s)
 ----- = Cell Motion (295.3deg/27.4 m/s)
 - . - . - = Propagation Vector(124.1 deg/22.4 m/s)

Plotted using wind shear 850-300mb

Using station: 72456
 72451
 72553

06-16-1992 00 UTC

Figure 50. Propagation vector plot for 16 June 1992 MCS.



_____ = Storm Motion (262.3deg/6.3 m/s)
 ----- = Inflow Motion (211.0deg/12.3 m/s)
 - . - . - = SR Inflow Vector(180.5 deg /9.7 m/s)

Using station: 72456

06-16-1992 00 UTC

Figure 51. Storm-relative inflow vector plot for 16 June 1992 for Topeka, KS.



_____ = Storm Motion (262.3deg / 6.3 m/s)
 - - - - - = Inflow Motion (214.3deg / 15.8 m/s)
 - . - . - = SR Inflow Vector (192.3 deg / 12.5 m/s)
 Using station: 72451
 06-16-1992 00 UTC

Figure 52. Same as in Fig. 51, except for Dodge City, KS.



_____ = Storm Motion (262.3deg / 6.3 m/s)
 - - - - - = Inflow Motion (200.0deg / 14.0 m/s)
 - . - . - = SR Inflow Vector (173.3 deg / 12.4 m/s)
 Using station: 72357
 06-16-1992 00 UTC

Figure 53. Same as in Fig. 51, except for Norman, OK.

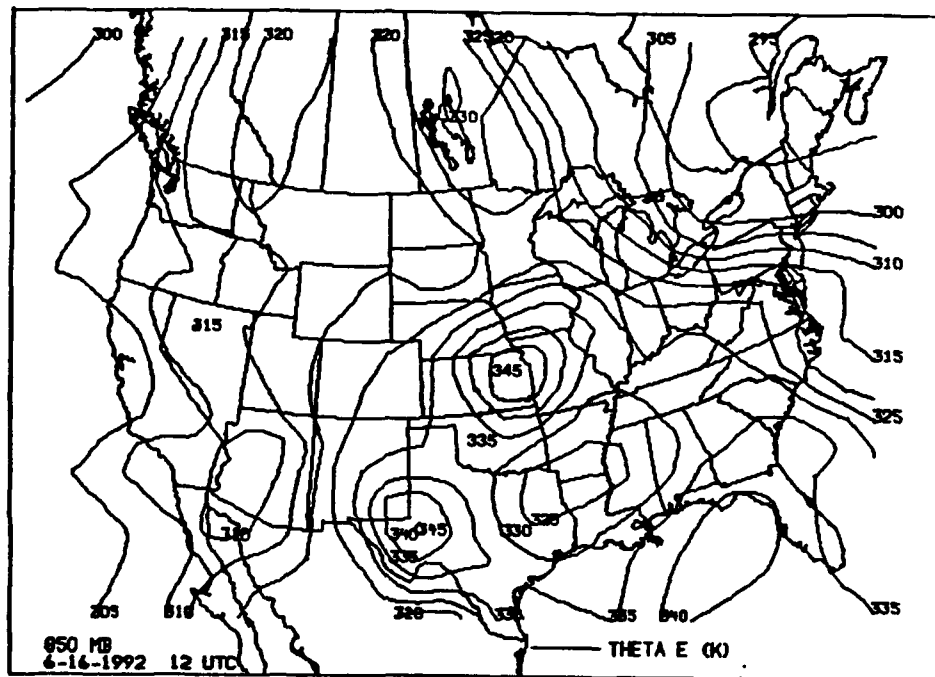


Figure 54. 850 mb θ_e for 12 UTC 16 June 1992.

far either. This adds credibility to the above reasoning. Aside from thunderstorm-scale factors contributing to storm propagation, another source of deviate motion may lie in the preexisting synoptic and subsynoptic boundary layer features (Weaver 1979) which appeared to play a major role in this case study.

As seen in the satellite imagery, the western edge of the MCS moved only slightly to the east-southeast which is an important indicator of the possible strength of the boundary layer convergence zone.

5. COMPOSITE RESULTS

Although the sample size of MCS events collected and archived in this study is not large, statistically, we observed several common characteristics for each propagation mode. The results are presented here.

a. Deviation of Storm Motion from Mid-Tropospheric Mean Wind and Wind Shear

We computed the deviation of the storm motion from the 850-300 mb average wind and wind shear in the u and v directions using the following equations:

$$V_{DEV} = V_{STORM} - V_{AVG} \quad (3)$$

$$V_{DEV} = V_{STORM} - V_{SHR} \quad (4)$$

Where: V_{DEV} is the deviation of the wind in the u or v direction;

V_{STORM} is the u and v components of storm motion;

V_{AVG} is the u and v components of the 850-300 mb average wind; and

V_{SHR} is the u and v components of the 850-300 mb wind shear.

This was done in order to calculate whether each MCS had a storm motion which was oriented to the right or left, and faster or slower than the mid-tropospheric mean wind or wind shear.

Results tended to show that storm motion was better described by the 850-300 mb average wind rather than wind shear. The $u_{\text{DEVIATION}}$ VS $v_{\text{DEVIATION}}$ for the small MCSs were plotted on a scatter diagram (Fig. 55). Upon inspection, it is evident that the storm motion deviation data points of the small MCSs exhibited were more organized when the 850-300 mb average wind was used (in other words, a "tighter" pattern). This was also the case for the large MCSs, forward, and backward propagating MCSs (not shown).

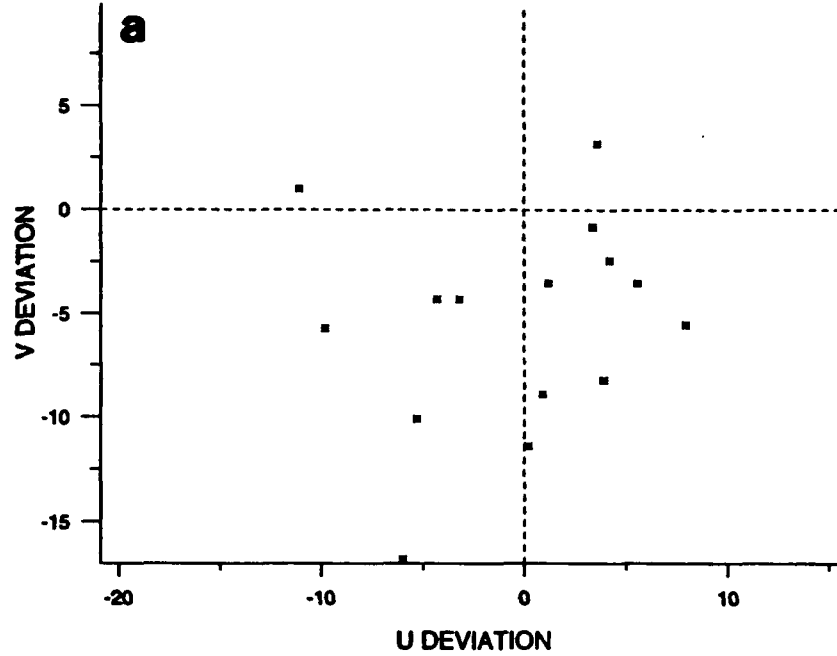
b. Computed Propagation Vectors vs Observed Propagation

In an effort to determine the accuracy of the computed propagation vectors from each MCS case, comparisons were made between the observed MCS propagation estimated by visually inspecting the satellite imagery and the computed propagation using the 850-300 mb average wind and wind shear.

Table 4 displays: storm, date and time, the size, the type of propagation, and the propagation direction of the MCSs. The propagation vectors were computed using the 850-300 mb average wind. All but one of these storms was classified as some type of a forward propagating MCS. This seems to suggest that the observed propagation of the majority of the forward propagating MCSs in this table were described best by the 850-300 mb average wind. Although there appears to be no size dependency, 10 of the 16 MCSs in Table 4 were classified as small.

The same type of data is displayed in Table 5 as in Table 4, but the propagation vectors were computed using the 850-300 mb wind shear. About

SMALL MCS DEVIATIONS USING STORM MOTION & 850-300 mb AVERAGE WIND



SMALL MCS DEVIATIONS USING STORM MOTION & 850-300 mb WIND SHEAR

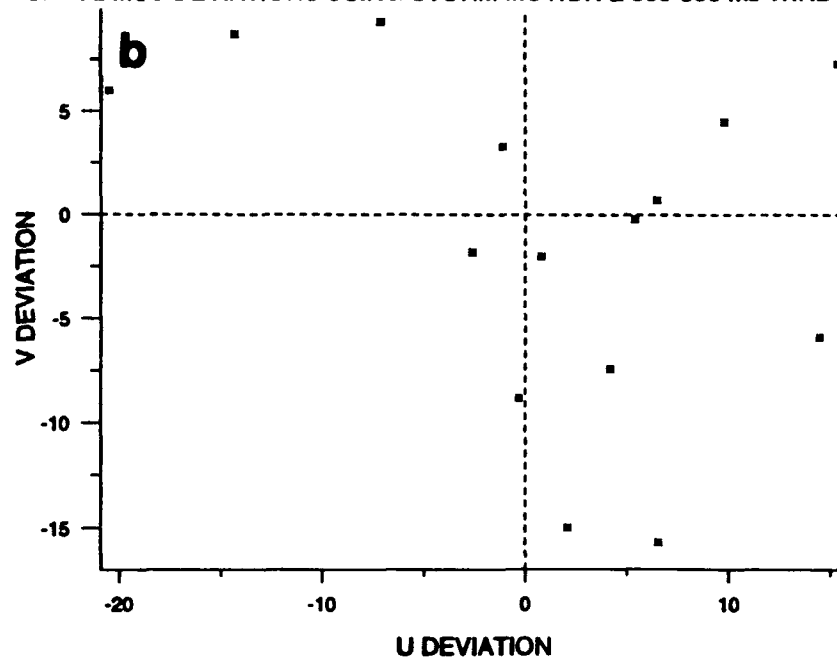


Figure 55. (a) Scatter diagram for the deviation of the storm motion from the 850-300 mb average wind. Axes are deviations in the u and v directions (b) same as in (a), except for 850-300 mb wind shear.

Table 4

Computed Storm Propagation Using Average Wind 850-300 mb vs Observed Propagation				
Storm	Date/Time (UTC)	Size S/L	Type of Propagation	Propagation Comp/Obs *
OK Storm	3 Sep 92/00	S	B-REL	045/060
OK Storm	9 Sep 92/00	S	Q-S	104/080
AR Storm	9 Sep 92/00	S	FWD	305/330
MI Storm	2 Jul 91/00	S	FWD	335/330
OH Storm	2 Jul 91/00	S	FWD	283/360
IL Storm	2 Jul 91/00	S	FWD	354/340
SD Storm	16 Jun 92/00	L	FWD	248/230
AR Storm	16 Jun 91/00	L	FWD	269/260
N TX Storm	21 Sep 92/00	S	FWD	300/030
S TX Storm	21 Sep 92/00	S	FWD	341/260
** Storm	5 Jun 91/12	L	FWD	345/340
** Storm	14 Sep 92/12	L	FWD	285/340
** Storm	18 Jun 92/00	S	B-REL	020/010
** Storm	10 Jul 91/12	L	H-FWD	070/100
** Storm	25 Jun 92/12	L	H-FWD	060/140
** Storm	16 Jun 91/00	S	FWD	302/280

* = Propagation in degrees. Direction propagating from.

Comp = Computed; Obs = Observed

** = Un-named storm

B-REL: Backward-Relative; Q-S: Quasi-Stationary; H-FWD: Hybrid-Forward

Table 5

Computed Storm Propagation Using Wind Shear 850-300 mb vs Observed Propagation				
Storm	Date/Time (UTC)	Size S/L	Type of Propagation	Propagation Comp/Obs *
ARKLA Storm	21 Sep 92/12	S	B-REL	330/290
NE OK Storm	10 Sep 92/12	L	H-BWD	058/045
TX Storm	11 Sep 92/00	L	BWD	083/070
TX Storm	3 Sep 92/00	S	FWD	002/340
IL Storm	9 Sep 92/12	L	FWD	220/230
IA Storm	9 Sep 92/12	S	B-REL	264/280
OH Storm	10 Sep 92/00	S	FWD	245/250
KS Storm	16 Jun 92/00	L	Q-S	124/120
OK Storm	16 May 90/00	L	B-REL	118/130
IL Storm	16 May 90/00	L	B-REL	225/260
** Storm	19 Jun 92/00	S	Q-S	106/120
** Storm	25 Jun 92/00	L	H-BWD	059/020

* = Propagation in degrees. Direction propagating from.

Comp = Computed; Obs = Observed.

** = Un-named storm.

B-REL: Backward-Relative; H-BWD: Hybrid-Backward

Only 28 of the 33 originally archived MCS cases are presented here. Five cases were not included due to undistinguishable propagation patterns on satellite imagery.

half of the MCSs detailed in Table 5 displayed a type of backward propagation (hybrid-backward, quasi-stationary, or backward). A majority of those storms were classified as large MCSs. These results suggest that large, backward propagating MCSs may best be described by the 850-300 mb wind shear vector.

The storm motion for each MCS was compared to the 850-300 mb average wind (Table 6) and wind shear (Table 7). None of the MCSs in Table 6 had a storm motion which was to the left of the direction of the average wind (looking downwind of the average wind). In fact, 10 of the 16 MCSs had a storm motion which was less than 30° to the right of the average wind, and 15 of the 16 MCSs had a storm motion which was less than 60° to the right. A majority of the MCSs in Table 6 (10 of 16) had a storm motion which was faster than the average wind (meaning there was forward propagation). However, in Table 7, there seems to be less consistency of the data, possibly suggesting that the motion of these storms would have been more difficult to forecast. In Table 7, only 4 of the 12 MCSs had a storm motion which was 30° or less to the right of the wind shear, with four MCSs having storm motions to the left of the wind shear. Also, 3 of the 12 MCSs had storm motions which were more than 60° to the left or right of the wind shear.

1. Synoptic Environments for Propagation Modes

The data in this section is presented in tabular form for ease of reading. Environmental parameters which may affect the propagation modes of MCSs are detailed here.

Table 6

Comparison of Storm Motion with 850-300 mb Average Wind for the Angle Between the Vectors, if Storm Motion Right (R) or Left (L) of Average Wind, and if Storm Motion is Faster (F), Slower (S) or Equal (=) to Average Wind						
Storm	Date/Time (UTC)	Size S/L	Type of Propagation	Storm Motion* vs Avg Wind Δ / R,L / F,S,=		
OK Storm	3 Sep 92/00	S	B-REL	28°	R	S
OK Storm	9 Sep 92/00	S	Q-S	0	-	=
AR Storm	9 Sep 92/00	S	FWD	27	R	F
MI Storm	2 Jul 91/00	S	FWD	27	R	F
OH Storm	2 Jul 91/00	S	FWD	0	-	F
IL Storm	2 Jul 91/00	S	FWD	35	R	F
SD Storm	16 Jun 92/00	L	FWD	32	R	F
AR Storm	16 Jun 91/00	L	FWD	10	R	F
N TX Storm	21 Sep 92/00	S	FWD	13	R	F
S TX Storm	21 Sep 92/00	S	FWD	15	R	=
** Storm	5 Jun 91/12	L	FWD	59	R	F
** Storm	14 Sep 92/12	L	FWD	26	R	F
** Storm	18 Jun 92/00	S	B-REL	47	R	S
** Storm	10 Jul 91/12	L	H-FWD	33	R	S
** Storm	25 Jun 92/12	L	H-FWD	124	R	=
** Storm	16 Jun 91/00	S	FWD	11	R	F

* = Angles are determined by looking downwind of 850-300 mb Avg Wind

** = Un-named storm

B-REL: Backward-Relative; Q-S: Quasi-Stationary; H-FWD: Hybrid-Forward

Table 7

Comparison of Storm Motion with 850-300 mb
Wind Shear for the Angle Between the Vectors, if Storm
Motion Right (R) or Left (L) of Wind Shear, and if Storm
Motion is Faster (F), Slower (S) or Equal (=) to Wind Shear

Storm	Date/Time (UTC)	Size S/L	Type of Propagation	Storm Motion* vs Wnd Shr Δ / R,L / F,S, =		
ARKLA Storm	21 Sep 92/12	S	B-REL	44°	R	F
NE OK Storm	10 Sep 92/12	L	H-BWD	61	R	S
TX Storm	11 Sep 92/00	L	BWD	143	R	F
TX Storm	3 Sep 92/00	S	FWD	37	R	F
IL Storm	9 Sep 92/12	L	FWD	69	L	F
IA Storm	9 Sep 92/12	S	B-REL	0	-	F
OH Storm	10 Sep 92/00	S	FWD	13	R	F
KS Storm	16 Jun 92/00	L	Q-S	33	L	S
OK Storm	16 May 90/00	L	B-REL	16	L	S
IL Storm	16 May 90/00	L	B-REL	29	L	F
** Storm	19 Jun 92/00	S	Q-S	50	R	S
** Storm	25 Jun 92/00	L	H-BWD	47	R	=

* = Angles determined by looking downwind of Wind Shear

** = Un-named storm.

B-REL: Backward-Relative; H-BWD: Hybrid-Backward

FORWARD PROPAGATION

<u>Max CAPE</u>	<u>Frontal Boundary</u>	<u>850 mb θ_e Ridge Axis</u>	<u>Vertical Motion</u>
Located near, S SE or SSW of MCS. CAPE Max normally $> 1000 \text{ J kg}^{-1}$ but not a requirement.	Position and type vary. May be a E-W Q-S STNRY front or an outflow bndry or a strong cold/warm front.	Ridge axis located S, SE, E or through the MCS. Max θ_e temperature S-SE of MCS.	In most cases weak PVA or weak NVA at 500 mb. Short wave with moderate PVA may or may not be present.
<u>Upper Level Wind Flow</u>	<u>Low Level Wind Flow</u>	<u>Avg Wind 700-300 mb</u>	<u>850-300 mb Thickness</u>
300 mb jet oriented E-W or SW-NE and positioned N W or NW of Does not always cross LLJ at large angles. Jet not always present.	If a max wind at 850 mb (LLJ) present, axis will be SE S SSW or OVHD the MCS. In some cases no low level wind max noted.	Strong winds (usually ~ 700 mb) may aid in its forward propagation of a MCS. Average wind speed was 32 knots.	Thickness gradient varies. MCS tended to move along contours but not always. Most MCSs near or in a thickness ridge. Not present all the time.

BACKWARD PROPAGATION

<u>Max CAPE</u>	<u>Frontal Boundary</u>	<u>850 mb θ_e Ridge Axis</u>	<u>Vertical Motion</u>
Positioned usually W SW or S of MCS. Strong CAPE may or may not be near MCS. Highest CAPE positioned S or on surface boundary.	Low level front appears to be necessary most of the time. Oriented E-W and STNRY or Q-S. Low level flow often normal to boundary. Max CAPE located on or S of boundary.	Ridge axis mostly to the NW W or SW of MCS, but S and SE noted as well. Max θ_e located S SW of MCS in most cases studied.	500 mb positive vorticity center may not be present. Weak NVA or zero vorticity advection upstream from MCS.
<u>Upper Level Wind Flow</u>	<u>Lower Level Wind Flow</u>	<u>Avg Wind 700-300 mb</u>	<u>850-300 mb Thickness</u>
300 mb ULJ usually weak and to the north of the MCS. Jet core usually well N-NW or NE of MCS. Jet axis configured as a trof.	850 mb LLJ may be oriented normal to SFC boundary. Direction varies. LLJ may or may not transport unstable air into MCS region.	Weak winds generally above the LFC (~ 700 mb) with the average wind speed was 20 knots.	Thickness diffluence noted NW or W of MCS with a moderate to strong thickness gradient N or NE of diffluence. MCS may or may not travel into thickness diffluence.

Also noted that the maximum Q-Vector convergence was usually located north or northeast of the MCS position.

QUASI-STATIONARY PROPAGATION

<u>Max CAPE</u>	<u>Frontal Boundary</u>	<u>850 mb θ_e Ridge Axis</u>	<u>Vertical Motion</u>
Highest CAPE located S or SE of MCS. Max CAPE may be located on or just south of a surface boundary and may not be near the MCS location.	Surface frontal boundary oriented E-W and stationary. MCS located S or on the frontal boundary.	Ridge axis located W SW S or through the MCS position. Max θ_e temperature SW or S of MCS.	Weak at best. Slight NVA to neutral vorticity advection upstream from MCS. Other sources of lift may be warm air advection or SFC boundary.
<u>Upper Level Wind Flow</u>	<u>Lower Level Wind Flow</u>	<u>Avg Wind 700-300 mb</u>	<u>850-300 mb Thickness</u>
300 mb ULJ generally oriented E-W with some cyclonic or anti-cyclonic curvature. Jet core well W-NW or N of MCS. Intersects LLJ at high angles W NW or N of MCS. Speeds moderate to strong.	850 mb LLJ oriented N-S. Will usually aid transport of highly unstable air to MCS region. Speeds moderate. May amplify overnight from 00 to 12 UTC. Often normal to surface boundary.	Moderate winds above LFC (~ 700 mb). Avg wind speed 36 knots.	Weak to slightly moderate thickness gradient over and N of MCS with varied thickness diffluence. May be thickness diffluence downstream from MCS.

Also noted moderate to strong Q-Vector convergence west or northwest of the MCS. Strongest Q-Vector convergence was positioned in the nearest moderate-to-strong thickness gradient west or northwest of the MCS.

Results in this section agree, to a high degree, with the surface and upper air features associated with the types of MCSs detailed by Shi and Scofield (1987) and Juying and Scofield (1989). The former and latter studies employed 30 minute-interval satellite imagery to determine MCS propagation. In our research, only one hour-interval satellite imagery was available, yet our results are very similar to theirs. Shi and Scofield and Juying and Scofield focused mainly on forward and backward propagating MCSs to improve satellite-derived convective rainfall algorithms, where we focused on forward, backward, and quasi-stationary propagation characteristics of MCSs. Most of the features examined by the above researchers were also examined in our research, with the addition of the analysis of CAPE and the computation of S-R inflow vectors and propagation vectors.

2. Storm-Relative Inflow Vectors

As stated in Chapter three, storm-relative (S-R) inflow vectors were computed for each MCS case in an effort to characterize the environment towards which the MCS propagated.

The source regions of the majority of the S-R inflow vectors for the forward propagating MCSs were characterized by higher CAPE, (if not the maximum CAPE), than the immediate region around the MCS. This was also true for the 850 mb θ_e ridge axes in some cases. As a general rule, though, most of the case studies had S-R inflow vectors directed from a region of higher CAPE.

The S-R inflow vectors for the B-REL propagating MCSs were generally directed from the south or southeast, relative to the position of the MCS. The forward propagating MCSs had S-R inflow vectors directed from the northeast through the east to the south, relatively speaking. The hybrid-forward propagating MCS S-R inflow vectors appeared to have been from a more southwesterly direction perhaps indicating a tendency, at times, not to propagate solely in the forward direction.

The backward (which includes hybrid-backward) propagating MCSs had S-R inflow vectors which originated from regions of higher CAPE and/or θ_e that were south, south-southwest, or southwest of the MCS region. The S-R inflow vectors were again almost 180° opposite to the observed propagation vector.

To a lesser extent than the cases above, the same was generally true for the quasi-stationary propagating MCSs. The S-R inflow vectors opposed the observed propagation vectors at angles less than 180° , ranging from near 90° to close to 140° . However, the source regions for these vectors appeared to be areas with comparatively more unstable air.

The fact that in the majority of these case studies the computed S-R inflow vector, to a high degree, was opposite in direction to the observed propagation is quite promising. This was true for the forward type, backward type, and generally the quasi-stationary propagation modes. This may lead to the conclusion that quite possibly, MCS propagation may be forecast best by **first** examining the synoptic environment of the near-storm region and **then** computing a S-R inflow vector in order to determine in which direction the

MCS will propagate. The synoptic environment can be analyzed for the kinematic, thermodynamic, and stability parameters detailed in this work and by previous works.

6. ASSOCIATED ERRORS

Random errors associated with upper level wind measurements from rawinsondes can be as great as $\pm 10\%$ in the raw data. Random errors are due to the inherent errors attributed to a given process of measurement; they are unpredictable (Moore 1985). Belt and Fuelberg (1982) found for their study that a rawinsonde observation at 900 mb may be in error by 2.0 degrees and 1.1 m s^{-1} and at 100 mb, the observation may be in error by 15.0 degrees and 5.6 m s^{-1} . However, as the raw data is objectively analyzed, random errors are reduced in the data. The data associated with the surface observations contains much less random errors. These errors in surface and upper air data would impact derived parameters such as moisture convergence.

In this study, we assumed that the convective cell moved parallel to the 850-300 mb average wind or wind shear based on earlier works referenced in Chapter 2. However, there are instances when this assumption does not apply. The convective cell was often difficult to track using the one hour IR imagery available in this study. The "coldest" top may tend to "jump" around in position from image to image. The assumption that following the storm centroid as a good approximation for the position of the cell has been used before (Kane et al. 1987). The goal was to focus on the direction of the MCS propagation vector qualitatively. As others have pointed out in their research (e.g., Merritt and Fritsch 1984) the speed of the propagation vector is difficult to determine. However, our goal was to describe the general characteristics of the

environment towards which a MCS propagates. So for this effort the direction of the propagation was more important than its magnitude.

In tracking the MCSs with the GOES IR imagery, the temporal interval between consecutive images was one hour. This timestep between images is, at best, the largest acceptable interval. Thirty minutes, or less, between images would have been ideal for tracking the convective timescale interactions of the MCS environment. In a relatively few cases missing imagery added to time steps that were sometimes two hours long.

Identification of cells in the MCSs was also a problem in some cases. Large MCSs were accompanied by a great deal of anvil debris covering a usually large area. Individual cells sometimes could not be resolved if the debris obscured the view. However, smaller MCSs, as a whole, were accompanied by less anvil debris and individual cells were more recognizable in the IR imagery. But it must be noted that resolving individual cells on the IR imagery is often difficult.

MCS propagation in the IR satellite imagery cannot, as a rule, be discerned as precisely as with the higher resolution (both temporal and spatial) WSR-88D radar data. Nevertheless, towering cumulus, overshooting tops, outflow boundaries, and other features important to propagation dynamics are readily observable in the satellite imagery which are not usually detectable in the radar data (Juying and Scofield 1989).

7. SUMMARY and CONCLUSIONS

In an attempt to examine why MCSs exhibit a particular type of propagation, numerous case studies were undertaken. Three case studies were presented in detail to analyze/characterize the synoptic environment towards which the MCS propagates. The first study, a forward propagating MCS, demonstrated how the propagation was strongly influenced by the location of the source of high CAPE air and the θ_e ridge axes. The storm propagated toward this region. The second study, a backward propagating MCS, revealed how a surface frontal boundary, a 850 mb LLJ, and moist unstable air played different roles in affecting the exhibited propagation. The third study, a quasi-stationary propagating MCS, appeared to be "anchored" in some fashion to preexisting synoptic/subsynoptic boundary layer features. The behavior of this MCS is similar to that discussed by Weaver (1979).

When the storm motion deviation of the MCSs was compared to the 850-300 mb average wind and wind shear, results showed that storm motion was more accurately described by the average wind in that layer. The pattern of the data points on the scatter-diagram was "tighter".

The signature characteristics noted in each propagation mode were also compiled. The data is in good agreement with the work done by Scofield (1987, 1989). There does seem to be a certain synoptic setting which promotes a particular type of propagation. However, as pointed out earlier, each setting is slightly different, and storm-scale influences can often change the behavior

of a MCS rather drastically. A larger sample size may be needed.

The computed S-R inflow vectors showed a very high correlation between the low level source of the MCS "fuel" and the direction toward which the MCS propagated. In almost every case study, the inflow vectors tended to have at least a directional component from the "fuel" region, if not the entire vector directed anti-parallel to the propagation vector. This holds great potential in being able to forecast MCS propagation based on the synoptic setting.

The computed propagation vectors were, for 71% of the case studies, less than 30° in error from the visually determined propagation. Of the remaining case studies, three were off by 40° or less, and five were in error by 81° or less. In the sample size of this research, there seemed to be no size or propagation-mode dependency on the accuracy of the computed propagation vector. The data compiled suggests that possibly the forward propagating MCSs are better forecast by using the 850-300 mb average wind, while the backward propagating MCSs are best forecast using the 850-300 mb wind shear vector.

New observational technology is and will be aiding forecasters in the "diagnosis and trend" aspect of assessing storm potential. New datasets include WSR-88D radar imagery, wind profilers, aircraft-measured winds, cloud-to-ground lightning strike networks, and so on. Regional mesoscale networks of surface stations and upper-air soundings also may become available in the near future. Mesoscale observations from special research projects such as PROJECT STORM are essential for a better understanding of the interactions between meso- and synoptic scale and vice versa (Juying and Scofield 1989).

For instance, the vertical profile of latent heat release may affect storm propagation. According to the theoretical work of Roadcap and Rao (1993) latent heat released has an important role in the cloud band growth and propagation in tropical MCSs. If similar dynamics were to govern the MCSs in this study, stationary MCSs would result if latent heat is released significantly in the upper layers (300 mb). Propagating MCSs are likely to result if pronounced amounts of latent heat are released in the middle levels (700 mb). Satellite data with increased temporal coverage should be implemented as well. All these new data sources are helping to remove the broad temporal and spatial gaps in the operational data network. Development of more powerful computers and convective-scale numerical weather prediction models will aid in the assessment of the severe local storm and MCS environment.

The changing perceptions of the complex processes associated with development of severe storms and MCSs make the utility of fixed meteorological checklists problematic. However, some form of a data-management or priority list may be a necessity if the forecaster is to effectively use all the new data and techniques to arrive at more accurate and timely forecasts. As experience is gained, it should become possible to devise procedures for analysis which could lead to a forecaster anticipating the formation and intensification of a MCS and the decay of existing ones. Hopefully, this work is one more important step towards a more complete understanding of MCS propagation.

In future research on this topic available sources of more accurate data

should include WSR-88D radar data in order to identify the individual cells of the MCS and to track the direction of the propagation. Microwave satellite data should also be incorporated to identify the areas of heavy rainfall or convective rainfall estimation techniques should be employed. Wind profiler data should be used to supplement the upper air observations taken every 12 hours. The above data sources will introduce a much higher degree of accuracy to future research because of their increased spatial and temporal resolution.

BIBLIOGRAPHY

- Barnes, S.L., 1973: Mesoscale Objective Map Analysis Using Weighted Time Series Observations, NOAA Technical Memo ERL NSSL 62, 60pp.
- Bartels, D.L., and J.M. Skradsk, and R.D. Menard, 1984: Mesoscale Convective Systems: A Satellite-Data-Based Climatology, NOAA Technical Memo ERL ESG-8, Boulder, CO, 58pp.
- Bartels, D.L., and A.A. Rockwood, 1983: Internal Structure and Evolution of a Dual Mesoscale Complex, Preprints, 5th *Conference on Hydrometeorology*, Tulsa, OK, Amer. Meteor. Soc., 97-102.
- Belt, C. L., and H.E. Fuelberg, 1982: The Effects of Random Errors in Rawinsonde Data on Derived Kinematic Quantities, *Mon. Wea. Rev.*, **110**, 91-101.
- Blackadar, A.K., 1957: Boundary Layer Wind Maximum and Their Significance for Growth of Nocturnal Inversions. *Bull. Amer. Meteor. Soc.*, **38**, 283-290.
- Browning, K.A., 1964: Airflow and Precipitation Trajectories within Severe Local Storms Which Travel to the Right of the Winds. *J. Atmos. Sci.*, **21**, 634-639.
- Browning, K.A. (ed.), 1965a: A Family Outbreak of Severe Local Storms--A Comprehensive Study of the Storms in Oklahoma on 26 May 1963. Part I, Report#AFCRL-65-695(I), Office of Aerospace Research, USAF Bedford, MA.
- Browning, K.A., and F.F. Hill, 1984: Structure and Evolution of a Mesoscale Convective System near the British Isles. *Quart. J. Roy. Meteor. Soc.*, **110**, 897-913.
- Chappell, C.F., 1986: *Mesoscale Meteorology and Forecasting*, P.S. Ray Ed., Amer. Meteor. Soc., 289-310.

- Clark, J.D., 1983: *GOES User's Guide*, U.S. Dept. of Commerce, Washington, D.C., 90pp.
- Colquhoun, J.R., 1975: A Method for Estimating the Velocity of Severe Thunderstorms. *Australian Meteor. Mag.*, 23, 99-107.
- Doswell, C.A., 1985: The Operational Meteorology of Convective Weather Volume II: Storm Scale Analysis, NOAA Technical Memo ERL ESG-15, Boulder, CO, 240pp.
- Doswell, C.A., 1987: The Distinction Between Large Scale and Mesoscale Contributions to Severe Convection: A Case Study Example. *Wea. Forecasting*, 2, 3-16.
- Doswell, C.A., and M. Splitt, 1991: On Storm Motion and Operational Assessment of Supercell Potential Using Hodographs, Preprints, 4th *Conference on Operational Meteorology*, Whistler British Columbia, Canadian Met. and Oceanographic Society, 245-253.
- Fawbush, E.J., and R.C. Miller, 1953: A Method for Forecasting Hailstone Size at the Earth's Surface. *Bull. Amer. Meteor. Soc.*, 35, 14-19.
- Follansbee, W.A., and V.J. Oliver, 1975: A Comparison of IR Imagery and Video Pictures in the Estimation of Daily Rainfall from Satellite Data, NOAA Technical Memo NESS 62, Washington, D.C., 14pp.
- Fritsch, J.M., and R.J. Kane, and C.R. Chelius, 1986: The Contribution of Mesoscale Convective Weather Systems to the Warm Season Precipitation in the United States. *J. Appl. Meteor.*, 25, 1333-1345.
- Funk, T.W., 1991: Forecasting Techniques Utilized by the Forecast Branch of the National Meteorological Center During a Major Convective Rainfall Event. *Wea. Forecasting*, 6, 548-564.

- Johns, R.H., and C.A. Doswell, 1992: Severe Local Storms Forecasting. *Wea. Forecasting.*, **7**, 588-612.
- Juying, X., and R.A. Scofield, 1989: Satellite-Derived Rainfall Estimates and Propagation Characteristics Associated with MCSs, NOAA Technical Memo NESDIS 25, Washington, D.C., 49pp.
- Kane, R.J., and C.R. Chelius, and J.M. Fritsch, 1987: Precipitation Characteristics of Mesoscale Convective Weather Systems. *J. Appl. Meteor.*, **26**, 1345-1357.
- Klemp, J.B., and R.B. Wilhelmson, 1978: The Simulation of Three-Dimensional Convective Storm Dynamics. *J. Atmos. Sci.*, **35**, 1070-1096.
- Klemp, J.B., and R.B. Wilhelmson, 1978: Simulations of Right- and Left-Moving Storms Produced Through Storm Splitting. *J. Atmos. Sci.*, **35**, 1097-1110.
- Maddox, R.A., 1980: Mesoscale Convective Complexes. *Bull. Amer. Meteor. Soc.*, **61**, 1374-1387.
- Maddox, R.A., 1981: The Structure and Life-Cycle of Mesoscale Convective Complexes, *Atm. Sci.*, Paper Number 336, Colorado State University, Ft. Collins, CO, 311pp.
- Maddox, R.A., 1983: Large-Scale Meteorological Conditions Associated with Mid-Latitude Mesoscale Convective Complexes. *Mon. Wea. Rev.*, **111**, 1475-1492.
- Maddox, R.A., and C.A. Doswell, 1982: An Examination of Jet Stream Configurations, 500 mb Vorticity Advection and Low Level Thermal Advection Patterns During Extended Periods of Intense Convection. *Mon. Wea. Rev.*, **110**, 184-197.

- Merritt, J.H., and J.M. Fritsch, 1984: On the Movement of Heavy Precipitation Areas of Mid-Latitude Mesoscale Convective Complexes, Preprints, 10th *Conference on Weather Forecasting and Analysis*, Clearwater, Amer. Meteor. Soc., 529-536.
- Miller, R.C., 1972: Notes on Analysis and Severe Storm Forecasting Procedures of the Air Force Global Weather Central, AWS TR200 (REV), Air Weather Service, Scott AFB, IL, 190pp.
- Moore, J.T., 1985: A Case Study of the Effects of Random Errors in Rawinsonde Data on Comparisons of Ageostrophic Winds. *Mon. Wea. Rev.*, 113, 1633-1643.
- Moore, J.T., and F. Glass, 1992: Mesoscale Convective Systems: Initiation and Propagation, Preprints, 4th *Conference on Operational Meteorology*, Whistler, British Columbia, Canadian Met. and Oceanographic Society, 215-224.
- Newton, C. W., 1960: Hydrodynamic Interactions with Ambient Wind Field as a Factor in Cumulus Development, Cumulus Dynamics, Proc. First *Conference on Cumulus Convection*, Oxford, 135-144.
- Newton, C.W., and J.C. Frankhauser, 1964: On the Movements of Convective Storms, with Emphasis on Size Discrimination in Relation to Water-Budget Requirements. *J. Appl. Meteor.*, 3, 651-668.
- Newton, C.W., and J.C. Frankhauser, 1975, Movement and Propagation of Multicellular Convective Storms. *Pageoph*, 113, 747-764.
- Newton, C.W., and S. Katz, 1958: Movement of Large Convective Rainstorms in Relation to Winds Aloft. *Bull. Amer. Meteor. Soc.*, 39, 129-136.

- Newton, C.W., and H.R. Newton, 1959: Dynamical Interactions Between Large Convective Clouds and Environments with Vertical Shear. *J. of Meteor.*, 16, 483-496.
- Rao, G.V., and A. Aksakal, 1992: Characteristics of Convection over the Arabian Sea During a Period Of Monsoon Onset, Submitted to *J. Atmos. Res.*, for future publication, 21pp.
- Roadcap, J.R., and G.V. Rao, 1991: A Linear Analysis of Monsoon Base States Associated with Banded Convection. Part I: Theory and Results. Accepted for Publication by the *Mon. Wea. Rev.*, in May 1993.
- Rolinski, T., and J.T. Moore, 1992: The Severe Convective Storms of 14-16 May 1990. *Nat. Wea. Dig.*, 17, 2-17.
- Shi, J., and R.A. Scofield, 1987: Satellite Observed MCS Propagation Characteristics and a 3-12 Hour Precipitation Forecast Index, NOAA Technical Memo NESDIS 20, Washington, D.C., 43pp.
- Uccellini, L.W., and D. Johnson, 1979: On the Coupling of Upper and Lower Tropospheric Jet Streaks and Implications for the Development of Severe Convective Storms. *Mon. Wea. Rev.*, 107, 682-703.
- Weaver, J.F., 1979: Storm Motion as Related to Boundary Layer Convergence. *Mon. Wea. Rev.*, 107, 612-619.
- Weisman, M.L., and J.B. Klemp, 1986: Characteristics of Isolated Convective Storms, *Mesoscale Meteorology and Forecasting*, Peter S. Ray ED., Amer. Meteor. Soc., 331-358.
- Zipser, E.J., 1982: Use of a Conceptual Model of the Life Cycle of Mesoscale Convective Systems to Improve Very Short Range Forecasts, *NOWCASTING*, F.A. Browning, ED., Academic Press, 256pp.

Vita Auctoris

Captain Charles H. Pappas was born in Bay Shore, New York in 1964. He attended New York Public schools until high school graduation in 1982. In 1982 he entered the Pennsylvania State University where he received his Bachelor of Science degree in 1986 majoring in meteorology and a commission into the Air Force.

His first assignment was as a Wing Weather Officer at McConnell Air Force Base, Kansas for the 384th Air Refueling Wing and 384th Bombardment Wing. In 1989, he was transferred to Det 25, 5WW where he served as the Officer-in-Charge of the Cadre Weather Team for the 193rd Light Infantry Brigade, Fort Clayton, Panama.

Captain Pappas is married to the former Amy Ann Miller from Davenport, Iowa, who is currently assigned to the 375th Airlift Wing at Scott Air Force Base, Illinois, as the Wing Commander's Executive Officer.